

Evaluating the blast-wave model as a description of 5 TeV p -Pb p_t spectra

Thomas A. Trainor

University of Washington, Seattle, WA 98195

(Dated: June 17, 2022)

The blast-wave (BW) spectrum model is interpreted to reveal relativistic motion (collective flow) of the hadron emission system relative to the center-of-momentum (CM) frame in high-energy A-B collisions. In essence, any spectrum deviation in the CM frame from a reference distribution (e.g. Boltzmann distribution on transverse mass m_t) is interpreted to reveal a flowing particle source. The ALICE collaboration has applied the BW model to identified hadron (PID) spectra for four hadron species from 5 TeV p -Pb collisions. From model fits BW parameters T_{kin} (freeze-out temperature) and $\langle\beta_t\rangle$ (transverse speed) are inferred that suggest strong radial expansion in more-central p -Pb collisions. Such results from the small p -Pb collision system are counterintuitive given that strong radial expansion should be driven by large density gradients. The present study is intended to address that problem. Several methods are employed to evaluate the quality of the BW model data description, including logarithmic derivatives and the Z-score statistic. The stability of the BW model definition across several applications to data is investigated. The BW model data description is compared to that of the two-component (soft+hard) model (TCM) that has been previously applied to the same p -Pb PID spectra. The general conclusion is that the BW model is falsified by p -Pb PID spectrum data according to standard statistical measures and that the fitted parameter values do not convey the intended meaning. Statistically acceptable data descriptions provided by the TCM indicate that other collision mechanisms (projectile-nucleon dissociation, dijet production), that are consistent with conventional QCD, are more likely responsible for observed spectrum characteristics.

I. INTRODUCTION

The blast-wave (BW) spectrum model has been widely applied to identified-hadron (PID) spectra from A-B collisions in the context of the high-energy heavy ion program whose central goal has been formation of a quark-gluon plasma (QGP). The basic premise is that BW spectrum analysis might confirm the presence of *radial flow* – radial expansion of a conjectured fluid assumed to be the dominant source of final-state particle emission. Initial application of the BW model to SPS β collisions (with $\sqrt{s_{NN}} \approx 19$ GeV) proved inconclusive [1]. However, early results from the relativistic heavy ion collider (RHIC) ($\sqrt{s_{NN}} \approx 130$ and 200 GeV) were interpreted to indicate the presence of significant radial flow (and hence QGP?), at least in more-central Au-Au collisions [2].

In motivating the RHIC experimental program it had been assumed that only for more-central A-A collisions involving the largest nuclei might the requisite energy and matter densities be generated to form a QGP. However, application of the BW model to smaller collision systems (e.g. p -A, d -A and even p - p) has led to claims that significant radial flow appears in all A-B collisions [3]. A recent example of the latter is BW analysis of PID spectra from 5 TeV p -Pb collisions [4]. Given the novelty and significance of such claims several questions emerge regarding BW model fits to PID spectra:

How well-defined is the theoretical basis for the BW model? That question goes beyond the basic Cooper-Frye formulation [5] relating particle emission in a relativistic moving frame to observed particle momenta in the center-of-momentum (CM) or laboratory (lab) frame. It concerns basic assumptions about the particle emission process – what does “particle emission” mean – and what

constraints does the emission environment (presumably high-density matter of uncertain nature) impose? Also, how consistent is the BW model formulation from one application to another? Can different research groups apply the *same* model to similar data and get the same result, or is each application unique and therefore unverifiable?

Regarding BW model fits to data what are the standards for concluding that a BW model (which one?) describes spectrum data with sufficient accuracy to *confirm* a flowing particle-source scenario? Does a *well-defined* BW model describe all available relevant data within *statistical* uncertainties. Is there a competing spectrum model that describes spectrum data qualitatively more accurately? Within the context of *prevailing practice* for applying the model is it possible to *falsify* the BW model?

To address those questions and other related considerations the following strategy is adopted: A reference model for comparison with BW results is introduced in the form of a two-component (soft + hard) model (TCM) applied to PID spectrum data from 5 TeV p -Pb collisions [6, 7]. A BW model description of the same PID data, as reported in Ref. [4], is reviewed. Several model-independent measures are employed to compare BW and TCM data descriptions. Limiting cases of the BW model are compared with a Boltzmann distribution (assuming thermal emission from a stationary particle source) and the TCM soft component (a limiting case corresponding to zero particle density and no jet contribution to spectra). Model fit quality is assessed with Z-scores based on published statistical and systematic data uncertainties.

To provide fuller context for model comparisons the concept of “two cultures” is introduced relating an approach based on perturbative QCD and parton cascades or showers on the one hand and an approach based on fluid-dynamic descriptions emerging from preQCD colli-

sion models on the other. Finally, the concept of “elementary collisions” as a reference is briefly considered with reference to particle data from p - p and e^+e^- collisions. Appendix A defines relativistic quantities appearing in BW derivations and reviews several BW model versions.

The goals of this study are: (a) understand the assumptions and formulations of the BW model as manifested by several versions, (b) assess whether underlying BW model assumptions are physically reasonable given present knowledge of QCD theory and improved data quality, (c) determine whether the BW model describes available data within uncertainties (statistical rather than systematic) or is falsified by data, and (d) consider an alternative spectrum model that appears superior as a data model and more physically interpretable.

This article is arranged as follows: Section II reviews a TCM description of PID spectrum data from 5 TeV p -Pb collisions reported in Ref. [4]. Section III briefly presents the BW model as it is applied to the same PID spectrum data. Section IV compares the shapes of the two spectrum models via several model-independent shape measures. Section V evaluates data fit quality for BW and TCM models using the Z-score statistical measure. Section VI provides a survey of BW model evolution over several decades. Section VII reviews systematic uncertainties. Sections VIII and IX present discussion and summary. Appendix A presents a detailed review of relativistic quantities and several BW model derivations.

II. TCM vs p-Pb PID SPECTRUM DATA

The two-component model (TCM) of PID hadron spectra described here provides a simple reference based on conventional soft and hard QCD processes that may furnish a better understanding of the BW model and its relation to spectrum data and collision dynamics. The PID spectrum data for seven charge-multiplicity n_{ch} classes from 5 TeV p -Pb collisions are as reported in Ref. [4]. Previous TCM analysis of those data is reported in Refs. [6–8]. A version of the PID TCM in which two parameters are varied with n_{ch} to accommodate spectrum data describes all data within their statistical uncertainties as demonstrated in Ref. [7].

A. p-Pb spectrum TCM for identified hadrons

The y_t spectrum TCM for *unidentified* hadrons is [8]

$$\begin{aligned}\bar{\rho}_0(y_t, n_s) &\approx \frac{d^2 n_{ch}}{y_t dy_t d\eta} \\ &= S(y_t, n_s) + H(y_t, n_s) \\ &\approx \bar{\rho}_s(n_s) \hat{S}_0(y_t) + \bar{\rho}_h(n_s) \hat{H}_0(y_t),\end{aligned}\quad (1)$$

where $y_t \equiv \ln[(m_t + p_t)/m_0]$ is transverse rapidity with $m_0 \rightarrow m_\pi$ assumed. $\hat{S}_0(y_t)$ and $\hat{H}_0(y_t)$ are unit-integral fixed model functions (independent of A-B centrality

or charge multiplicity n_{ch}), and $\bar{\rho}_s(n_s)$ and $\bar{\rho}_h(n_s)$ are soft and hard charge densities with $\bar{\rho}_x \equiv n_x/\Delta\eta$ and $\bar{\rho}_0 = \bar{\rho}_s + \bar{\rho}_h$. Soft yield n_s serves as a centrality index. A-B charge densities are defined in terms of N-N quantities by $\bar{\rho}_s = (N_{part}/2)\bar{\rho}_{sNN}$ and $\bar{\rho}_h = N_{bin}\bar{\rho}_{hNN}$ with $x \equiv \rho_{hNN}/\rho_{sNN}$ and $\nu \equiv 2N_{bin}/N_{part}$ and with $\bar{\rho}_h/\bar{\rho}_s = x(n_s)\nu(n_s)$. For linear superposition of N-N collisions in A-B collisions $\bar{\rho}_{hNN} \approx \alpha(\sqrt{s_{NN}})\bar{\rho}_{sNN}^2$ [8, 9].

Given the A-B spectrum TCM for unidentified hadron spectra a corresponding TCM for identified hadrons can be generated by assuming that each hadron species i comprises certain *fractions* of soft and hard TCM components denoted by $z_{si}(n_s)$ and $z_{hi}(n_s)$ assumed independent of y_t . The PID spectrum TCM is then expressed as [6, 7]

$$\bar{\rho}_{0i}(y_t, n_s) = S_i(y_t, n_s) + H_i(y_t, n_s) \quad (2)$$

$$\approx z_{si}(n_s)\bar{\rho}_s\hat{S}_{0i}(y_t) + z_{hi}(n_s)\bar{\rho}_h\hat{H}_{0i}(y_t, n_s)$$

$$\frac{\bar{\rho}_{0i}(y_t, n_s)}{z_{si}(n_s)\bar{\rho}_s} \equiv X_i(y_t, n_s) \quad (3)$$

$$\approx \hat{S}_{0i}(y_t) + \tilde{z}_i(n_s)x(n_s)\nu(n_s)\hat{H}_{0i}(y_t),$$

where $\tilde{z}_i(n_s) \equiv z_{hi}(n_s)/z_{si}(n_s)$ and unit-integral model functions $\hat{S}_{0i}(y_t)$ and $\hat{H}_{0i}(y_t)$ depend on hadron species i . Soft fraction $z_{si}(n_s)$ is expressed within the TCM by

$$z_{si}(n_s) = \left[\frac{1 + x(n_s)\nu(n_s)}{1 + \tilde{z}_i(n_s)x(n_s)\nu(n_s)} \right] z_{0i}, \quad (4)$$

where $z_{hi}(n_s) = \tilde{z}_i(n_s)z_{si}(n_s)$ and $\bar{\rho}_{0i} \equiv z_{0i}\bar{\rho}_0$ defines z_{0i} . Thus, if $\tilde{z}_i(n_s)$ and z_{0i} are specified for relevant hadron species then all of the PID TCM is determined. Model functions $\hat{S}_{0i}(y_t)$ are defined on proper m_{ti} for a given hadron species i and then transformed to $y_{t\pi}$. $\hat{H}_{0i}(y_t)$ are always defined on $y_{t\pi}$. The basis for the $\hat{S}_{0i}(y_t)$ model definitions is the limit of normalized spectra $X_i(y_t, n_s)$ as $n_{ch} \rightarrow 0$ (*zero particle density*). Soft-component models are thus always derived from data spectra. Inferred *data* spectrum hard components are then by definition the complement of *model* soft components so defined.

Properties of TCM soft-component models $\hat{S}_{0i}(m_t)$ are consistent with nuclear transparency in p -A collisions [10] and A-B collisions [11] and with the wounded-nucleon model [12]. Properties of TCM hard-component models $\hat{H}_{0i}(y_t)$ are consistent with measured properties of minimum-bias jets within A-B collisions if they consist of *linear superpositions* of N-N collisions [13–17].

B. 5 TeV p-Pb TCM model parameters

Table I presents TCM geometry parameters for 5 TeV p -Pb collisions inferred from the analysis in Ref. [18]. Those geometry parameters, derived from p -Pb p_t spectrum and ensemble \bar{p}_t data for unidentified hadrons [18–20], are assumed valid for each identified-hadron species (confirmed in Ref. [8]). $\bar{\rho}_0 = n_{ch}/\Delta\eta$ charge densities are measured quantities inferred from Fig. 16 of Ref. [21].

Relations $N_{bin} = N_{part} + 1$ and $\nu = 2N_{bin}/N_{part}$ involve number of nucleon N participants and N-N binary collisions. $\bar{\rho}_{sNN}$ is the mean soft-component charge density per participant pair averaged over all pairs. $x \equiv \bar{\rho}_{hNN}/\bar{\rho}_{sNN} \approx \alpha\bar{\rho}_{sNN}$ is the N-N hard/soft density ratio. Column σ'/σ_0 presents nominal centralities (bin centers) reported by Ref. [4] in connection with measured charge densities $\bar{\rho}_0$ whereas column σ/σ_0 presents values inferred in Ref. [18]. The remaining values in the table are results of the latter analysis.

TABLE I: TCM fractional cross sections σ/σ_0 (bin centers) and geometry parameters, midrapidity charge density $\bar{\rho}_0$, TCM N-N soft component $\bar{\rho}_{sNN}$ and N-N hard/soft ratio $x(n_s)$ used for 5 TeV p -Pb PID spectrum analysis [18]. Centrality parameters are from Ref. [18]. σ'/σ_0 values are from Table 1 of Ref. [4] as determined in Ref. [21].

| n | σ'/σ_0 | σ/σ_0 | N_{bin} | ν | $\bar{\rho}_0$ | $\bar{\rho}_{sNN}$ | $x(n_s)$ |
|-----|--------------------|-------------------|-----------|-------|----------------|--------------------|----------|
| 1 | 0.025 | 0.15 | 3.20 | 1.52 | 44.6 | 16.6 | 0.188 |
| 2 | 0.075 | 0.24 | 2.59 | 1.43 | 35.9 | 15.9 | 0.180 |
| 3 | 0.15 | 0.37 | 2.16 | 1.37 | 30.0 | 15.2 | 0.172 |
| 4 | 0.30 | 0.58 | 1.70 | 1.26 | 23.0 | 14.1 | 0.159 |
| 5 | 0.50 | 0.80 | 1.31 | 1.13 | 15.8 | 12.1 | 0.137 |
| 6 | 0.70 | 0.95 | 1.07 | 1.03 | 9.7 | 8.7 | 0.098 |
| 7 | 0.90 | 0.99 | 1.00 | 1.00 | 4.4 | 4.2 | 0.047 |

Table II presents hard-component model parameters based on optimized descriptions of spectrum hard components for the *most-central* ($n = 1$) p -Pb event class as described in Ref. [6]. TCM soft-component parameters remain unchanged from those reported in Table II of Ref. [6], with $(T, n) = (145 \text{ MeV}, 8.5)$, $(200 \text{ MeV}, 14)$ and $(210 \text{ MeV}, 14)$ for pions, kaons and baryons respectively. More-massive hadrons are less sensitive to exponent n . Those parameters and these in Tables I and II define a *fixed* PID TCM established as a reference. In Ref. [7] a *variable* TCM is defined wherein certain hard-component parameters (Gaussian widths σ_{y_t} below or above the hard-component mode or centroids \bar{y}_t) are varied linearly with centrality measure ν to accommodate data (see Fig. 4 of Ref. [7]). The variable TCM describes all spectra within statistical uncertainties as in Fig. 1.

C. 5 TeV p -Pb PID spectrum data

Identified-hadron spectrum data obtained from Ref. [4] for the present analysis were produced by the ALICE collaboration at the LHC. Collision events were divided into seven charge-multiplicity n_{ch} or p -Pb centrality classes based on yields in a VZERO-A (V0A) counter subtending $2.8 < \eta_{ab} < 5.1$ in the Pb direction. Hadron species include charged pions π^\pm , charged kaons K^\pm , neutral kaons K_S^0 , protons p and Lambdas Λ , $\bar{\Lambda}$.

Figure 1 shows PID spectrum data (densities on p_t) from Ref. [4] (points) plotted vs logarithmic variable y_t .

TABLE II: Revised PID TCM hard-component model parameters ($\bar{y}_t, \sigma_{y_t}, q$) for identified hadrons from 5 TeV p -Pb collisions derived from the differential spectrum analysis in Rev. [6]. Parameter z_{0i} values, inferred as limiting values of $z_{si}(n_s)$ centrality trends (Fig. 9 of Ref. [6]), are also included. Uncertainties are determined as one half the parameter change that would produce an obvious variation in $z_{hi}(y_t, n_s)$ ratios (e.g. Fig. 3 of Ref. [7]). Values with no uncertainties are duplicated from a related particle type.

| | \bar{y}_t | σ_{y_t} | q | z_{0i} |
|-----------|-------------------|-------------------|----------------|-------------------|
| π^\pm | 2.46 ± 0.005 | 0.575 ± 0.005 | 4.1 ± 0.5 | 0.82 ± 0.01 |
| K^\pm | 2.655 | 0.568 | 4.1 | 0.128 ± 0.002 |
| K_S^0 | 2.655 ± 0.005 | 0.568 ± 0.003 | 4.1 ± 0.1 | 0.064 ± 0.002 |
| p | 2.99 ± 0.005 | 0.47 ± 0.005 | 5.0 | 0.065 ± 0.002 |
| Λ | 2.99 ± 0.005 | 0.47 ± 0.005 | 5.0 ± 0.05 | 0.034 ± 0.002 |

That format (log-log with respect to p_t) provides detailed access to low- p_t structure (where most jet fragments appear) and clearly shows power-law trends at higher p_t . The curves are TCM parametrizations as reported above and demonstrated in Ref. [7] to describe spectrum data within their statistical uncertainties. As in Ref. [4] the spectra are scaled up by powers of 2 according to 2^{n-1} where $n \in [1, 7]$ is the centrality class index and $n = 1$ is *least* central (following the usage in Ref. [4]). In this paper $n = 1$ denotes the *most* central data as in Table I.

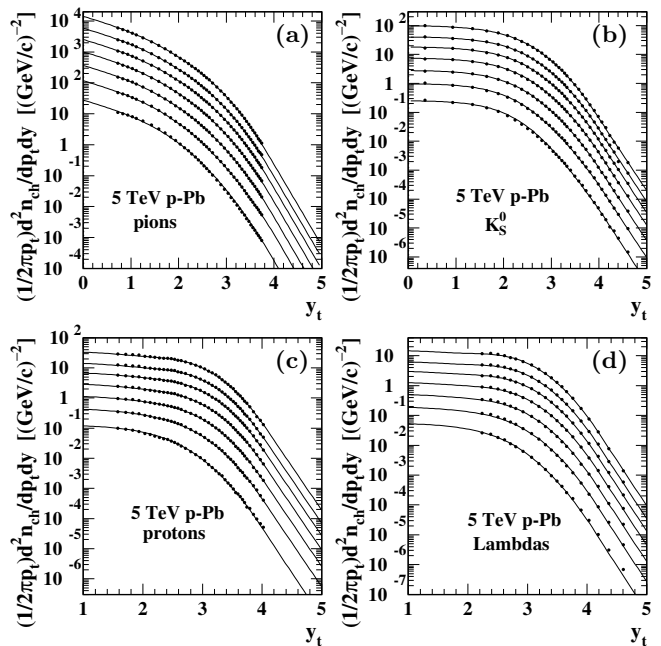


FIG. 1: p_t spectra for identified hadrons from 5 TeV p -Pb collisions [4] plotted vs pion transverse rapidity y_t (default) for: (a) pions, (b) neutral kaons, (c) corrected protons, (d) Lambdas. Solid curves represent the PID spectrum TCM from Ref. [7]. Proton inefficiency corrections are described in Ref. [6]. The statistical uncertainties (0.1 to 1% of data values, e.g. see Fig. 17) are all smaller than the point size.

Note that in the format of Fig. 1 a Boltzmann exponential on transverse mass m_t appears as $A - m_i \cosh(y_t)/T_i$, where m_i is the mass for hadron species i and A is a constant, and a power law on m_t appears as a straight line. The exception is for pion spectra including a substantial resonance contribution for $y_t < 2$ ($p_t < 0.5$ GeV/c) [6].

III. BW MODEL vs p-Pb PID SPECTRUM DATA

Reference [4] applies a blast-wave model to p_t spectrum data for 5 TeV V0A p -Pb spectra, with fit parameters reported in its Fig. 6. The BW fit parameters are mean radial speed $\langle\beta_T\rangle \rightarrow \bar{\beta}_t$, “kinetic freezeout” temperature T_{kin} and radial-speed $\beta_t(r)$ profile parameter n as in Table 5 of Ref. [4] (and see Table III below).

Application of certain fit models (e.g. BW models) to spectrum data for small collision systems has been invoked in a number of studies to claim presence of collectivity (flows) in such systems. For example, in Ref. [22] (reporting BW analysis of unidentified hadrons from p - p collisions) the BW model is said to be a “more standard description” and is “based on collective flow in small systems.” The BW model is said to be “quite good in explaining the bulk part of the system, however it fails at low- p_T below 0.5 GeV/c which could possibly be due to the decays of hadronic resonances.” “The applicability of [the BW model] is verified by fitting the transverse momentum spectra of the bulk part (~ 2.5 GeV/c)....”

TABLE III: Blast-wave parameters for simultaneous fits of pion, charged-kaon, neutral kaon, proton and Lambda spectra from 5 TeV p -Pb collisions [4]. The σ'/σ_0 values are the cross-section fractions (bin centers) reported in Ref. [4]. Table I shows alternative σ/σ_0 values determined in Ref. [18].

| n | σ'/σ_0 | $\langle\beta_T\rangle$ | T_{kin} (GeV) | n | χ^2/ndf |
|-----|--------------------|-------------------------|-----------------|------|---------------------|
| 1 | 0.025 | 0.547 | 0.143 | 1.07 | 0.27 |
| 2 | 0.075 | 0.531 | 0.147 | 1.14 | 0.33 |
| 3 | 0.15 | 0.511 | 0.151 | 1.24 | 0.36 |
| 4 | 0.30 | 0.478 | 0.157 | 1.41 | 0.35 |
| 5 | 0.50 | 0.428 | 0.164 | 1.73 | 0.43 |
| 6 | 0.70 | 0.36 | 0.169 | 2.4 | 0.54 |
| 7 | 0.90 | 0.26 | 0.166 | 3.9 | 0.84 |

The argument presented in Ref. [4] for applying the BW model to PID spectrum data and interpreting the result in a hydrodynamic context proceeds as follows:

(a) Low- p_t regions of hadron spectra convey important information: “The p_T distributions and yields of particles of different mass at low and intermediate momenta of less than a few GeV/c (where the vast majority of particles is produced) can provide important information about the system created in high-energy hadron reactions.”

(b) Hydrodynamics-based spectrum models (e.g. blast-wave model) provide useful data descriptions: “The measured p_T distributions are compared to...hydrodynamic

models.” “Several [spectrum] parametrizations have been tested, among which the blast-wave function...gives the best description of the data over the full p_T range... [model applied *individually* to different hadron species].”

(c) Spectrum trends for heavy-ion collisions appear to buttress validity of a blast-wave spectrum model: “In heavy-ion collisions, the flattening of transverse momentum distribution and its mass ordering find their natural explanation in the collective radial expansion of the system. This picture can be tested in a blast-wave framework with a simultaneous fit to all particles for each multiplicity bin. This parameterization assumes a locally thermalized medium, expanding collectively with a common velocity field and undergoing an instantaneous common freeze-out.” “This [collective hydrodynamic flow] results in a characteristic dependence of the [spectrum] shape which can be described with a common kinetic freeze-out temperature parameter T_{kin} and a collective average expansion velocity $\langle\beta_t\rangle$ [citing Ref. [1]].”

In referring to *simultaneous* BW fits to PID spectra Ref. [4] presents no BW-data fit residuals to support its very low χ^2 values (as reproduced in Table III). Claimed good agreement between *individual* BW fits and data appears to extend (for neutral kaons and Lambdas) up to 7 GeV/c where one might expect parton fragmentation to jets to produce essentially *all* detected hadrons. Why should the BW model have any relation to that p_t region?

The BW model used in Ref. [4] to fit spectrum data is adopted from Ref. [1] that introduced a hydrodynamics-based formula to describe pion spectra from 200 GeV fixed-target ($\sqrt{s_{NN}} \approx 19$ GeV) S-S collisions at the CERN SPS. The relevant formula is Eq. (7) of Ref. [1]

$$\frac{dn}{m_t dm_t} \propto m_t \int_0^R d\mathbf{f} \int_0^{\rho} \left[\frac{p_t \sinh(\rho)}{T} \right] K_1 \left[\frac{m_t \cosh(\rho)}{T} \right], \quad (5)$$

with boost $\rho = \tanh^{-1}(\beta_t)$ and transverse speed $\beta_t(r) = \beta_s (\mathcal{Y}R)^n$, where $n = 1$ corresponds to Hubble expansion, β_s is the expansion speed at the emitter surface and I_0 and K_1 are modified Bessel functions. The mean transverse speed is $\langle\beta_t\rangle \rightarrow \bar{\beta}_t = 2\beta_s/(n+2)$. Equation (5) then in effect represents a thermal (Boltzmann) energy spectrum in the boost (comoving) frame convoluted with a source boost (speed) distribution on source radius to describe the particle spectrum measured in the lab frame.

Figure 2 shows the same PID spectrum data from 5 TeV p -Pb collisions appearing in Fig. 1 (points) accompanied in this case by *simultaneous* BW fits to four hadron species (solid) with fit values corresponding to Table III. The various n_{ch} classes are scaled up by powers of 2 just as in Fig. 1. The BW model spectra have been scaled in this case to best agree with data spectra within the indicated BW fit intervals (arrows). cursory inspection suggests that the BW description of pion spectra is not relevant to interpretation. The BW descriptions of spectra for more-massive hadrons appear to accommodate data reasonably well below $y_t = 3-3.6$ ($p_t \approx 1.4-2.6$ GeV/c), but see Sec. V for detailed assessment of fit quality.

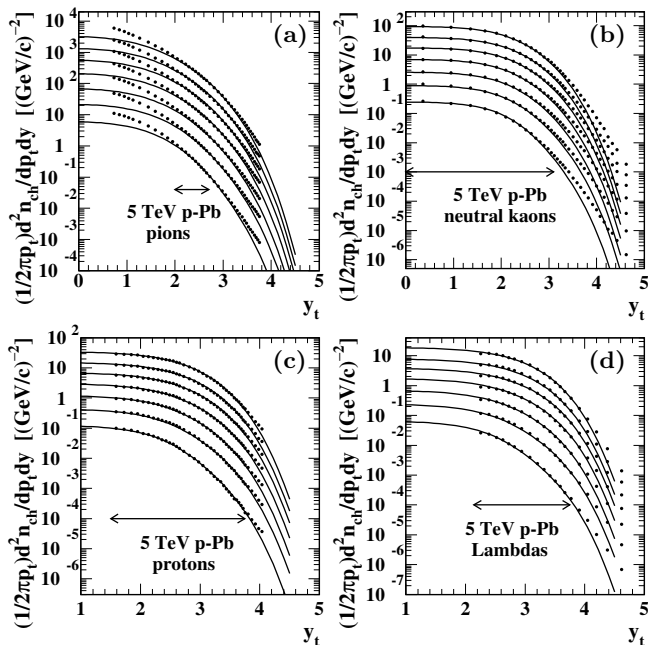


FIG. 2: p_t spectra for identified hadrons from 5 TeV p -Pb collisions [4] plotted vs pion transverse rapidity y_t (default) for: (a) pions, (b) neutral kaons, (c) corrected protons, (d) Lambdas. Solid curves represent blast-wave model fits from Ref. [4] with amplitudes adjusted here to best describe data within reported BW fit intervals (arrows).

IV. SPECTRUM MODEL COMPARISONS

The TCM provides absolute predictions for hadron yields as well as spectrum shapes. TCM predictions span n_{ch} or centrality variation within a given A-B collision system as well as variations from system to system (e.g. from p - p to p -Pb to Pb-Pb). In contrast, the BW model is not expected to provide such absolute predictions: “...the normalization of the spectrum...we will always adjust for a best fit to the data, because we are *only interested in the shape* of the spectra to reveal the dynamics of the collision zone at freeze-out [emphasis added]” [1]. Given those limitations any direct model comparisons must be based on shape measures that are not model dependent so as to provide unbiased results. Setting aside absolute yields how best can one demonstrate the evolution of spectrum shape, thus how best test model validity?

For what follows groups of spectra under comparison (e.g. n_{ch} variation for given hadron species) are rescaled so as to agree in amplitude near $p_t = 0$. The specific common value is not relevant. Successive differences between spectra are considered in relation to TCM hard-component model shapes. Integrals of high- p_t and low- p_t intervals (absolute yields) for variable-TCM representations of data spectra are examined. Given that TCM context, *ratios* of high- p_t to low- p_t intervals for both TCM and BW model are considered as a function of n_{ch} or centrality. Logarithmic derivatives (curvature measures) are

applied to TCM and BW models to provide differential spectrum shape information. Spectrum shape variations for each BW model parameter (with others held fixed) are examined in turn. Finally, the BW model is compared with a Boltzmann exponential and with TCM $\hat{S}_0(m_t)$.

A. Spectrum differences

Figure 3 shows data spectra (solid) for pions (left) and protons (right). The p_t acceptances are rather limited and thus not pursued further in this section. The TCM (dashed) describes data within their statistical uncertainties as demonstrated in Ref. [7] Sec. III E. TCM soft components $\hat{S}_0(y_t)$ (dotted) represent the limiting case for spectrum data with charge density $\bar{\rho}_0 \rightarrow 0$ (i.e. zero particle density). For pions (left) a second $\hat{S}_0(y_t)$ curve below the data at low y_t includes no correction for conjectured resonance contributions (see Sec. III A of Ref. [6]). Arrows in these and other panels indicate y_t intervals used for BW fits as reported in Ref. [4].

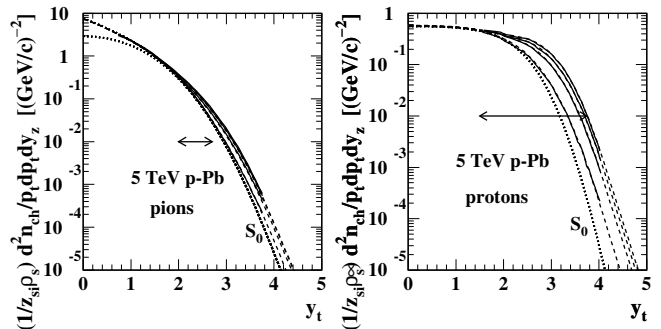


FIG. 3: Data spectra (densities on p_t) for identified pions and protons from 5 TeV p -Pb collisions [4] (solid curves) and corresponding TCM curves (dashed) for four centrality classes plotted on logarithmic transverse rapidity y_t . The spectra are rescaled to quantity $X_i(y_t)$ as defined in Eq. (3). For clarity only curves for centralities $n = 1, 3, 5, 7$ are plotted. The lower dotted $\hat{S}_0(y_t)$ curve for pions is without resonances.

Figure 4 shows spectrum data for neutral kaons (a) and Lambdas (c) with the same line styles as described above. Again the TCM describes data within their statistical uncertainties. The p_t acceptances are large in both cases, providing meaningful model tests below.

Figure 4 (c,d) show differences between spectra for a given n_{ch} class ($n = 1-6$) and spectra for the lowest n_{ch} class ($n = 7$) for each of neutral kaons (b) and Lambdas (d), and for data (solid) and TCM (dashed). The point of this exercise is to isolate spectrum “hard components” without resorting to *a priori* physical assumptions, thereby repeating the empirical procedure employed in Ref. [9] first used to establish the TCM for 200 GeV p - p collisions. As noted in that p - p analysis data structures so isolated are approximately independent of n_{ch} (e.g. p -Pb centrality), thus demonstrating that full spectra can be represented as superpositions of two fixed

model functions. The amplitude of one (hard) varies as the square of the other (soft) for each N-N collision.

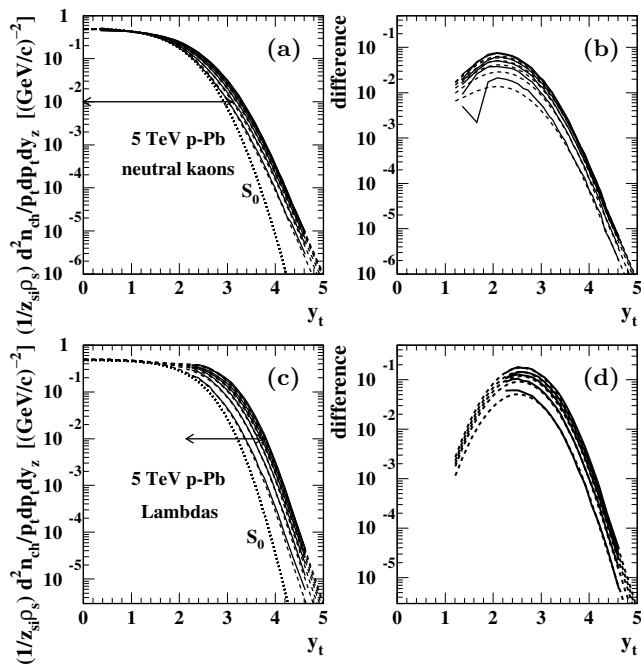


FIG. 4: Data p_t spectra for identified neutral kaons (a,b) and Lambdas (c,d) from 5 TeV p -Pb collisions [4] (solid curves) and corresponding TCM curves (dashed) for four centrality classes. Panels (a,c) compare rescaled data spectra (solid) to TCM (dashed). Panels (b,d) show differences between spectra for $n = 1 - 6$ and peripheral spectrum $n = 7$.

More specifically, modes of the “hard components” move from lower to higher y_t with increasing hadron mass such that spectra for various hadron species tend to coincide at high y_t (e.g. near $y_t = 5$ or $p_t \approx 10$ GeV/c). Baryon hard components also tend to fall more rapidly below the mode than mesons. Those trends are consistent with fragmentation functions for identified hadrons from e^+e^- collisions [13]. Systematic uncertainties below the mode for difference spectra in panels (b,d) are substantially greater than reported in Refs. [6, 7] because of the simpler method invoked here to reduce model dependence. Similar results are obtained by subtracting $\hat{S}_0(y_t)$ model functions (dotted) in the left panels.

Figure 5 shows pion (left) and proton (right) spectra from the BW model in Eq. (5) using fitted parameter values in Table III, both as reported in Ref. [4]. Soft-component model $\hat{S}_0(y_t)$ (dashed) at left does not include the conjectured resonance contribution that appears in Fig. 3 (left, upper dotted) and describes pion data. The BW curves (solid) have been rescaled to coincide near $y_t = 0$ with the $\hat{S}_0(y_t)$ soft-component curves (dashed).

Figure 6 (a,c) shows neutral kaon (a) and Lambda (c) spectra from the BW model in Eq. (5) using fitted parameter values in Table III, both as reported in Ref. [4].

Figure 6 (b,d) shows differences between BW spectra for a given n_{ch} class ($n = 1-6$) and spectra for the low-

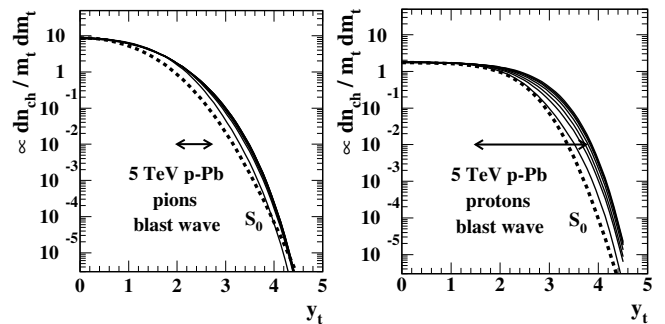


FIG. 5: Blast-wave model m_t spectra for identified pions and protons from 5 TeV p -Pb collisions [4] for seven centrality classes. The bold dashed curves are TCM soft-component model $\hat{S}_0(y_t)$. The curves are scaled to coincide at $y_t = 0$.

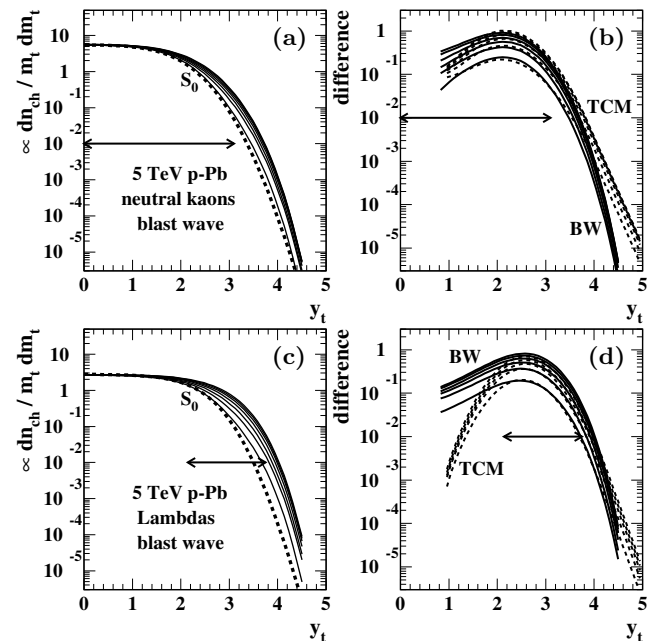


FIG. 6: Blast-wave model m_t spectra (solid) for identified neutral kaons (a,b) and Lambdas (c,d) from 5 TeV p -Pb collisions [4]. The bold dashed curves in (a,c) are TCM soft-component model $\hat{S}_0(y_t)$. Curves in (a,c) are scaled to coincide at $y_t = 0$. Panels (b,d) show differences (solid) between BW spectra for $n = 1 - 6$ and peripheral spectrum $n = 7$. Dashed curves in (b,d) are TCM dashed curves from Fig. 4 (b,d) that represent the data spectrum differences there. The TCM curves are all rescaled by the same factor to best correspond with BW curves within fit intervals (arrows).

est n_{ch} class ($n = 7$) for each of neutral kaons (b) and Lambdas (d). The dashed curves are TCM differences repeated from panels (b,d) of Fig. 4 to provide a reference. In either case the dashed curves have all been rescaled by the *same factor* to accommodate the solid BW curves.

This comparison highlights two issues: (a) The BW curves below the mode remain high while the TCM data representations fall more rapidly. That is especially obvious for the Lambda spectra since baryon hard compo-

nents have modes at higher y_t and are narrower compared to meson hard components [7]. (b) The BW curves above the mode fall off rapidly while the TCM data representations follow a power-law trend that is more gradual. That is especially obvious for the kaon spectra for the same reasons given above. The contrast is amplified by the different BW fit intervals used for the two cases.

B. High/low ratio centrality trends

Certain centrality trends are more interpretable when presented in the context of 5 TeV p -Pb centrality variation as reported in Ref. [18] based on accurate TCM description of ensemble \bar{p}_t data for that collision system. That centrality model then provided the basis for PID spectrum studies reported in Refs. [8], [6] and [7],

Figure 7 [Fig. 17 of Ref. [6] in relation to its Eqs. (26) and (27)] shows soft fraction $\bar{\rho}_s/\bar{\rho}_0$ (left) and hard/soft ratio $\bar{\rho}_h/\bar{\rho}_s \equiv x(n_s)\nu(n_s)$ (right) vs charge-density soft component $\bar{\rho}_s$, with $\bar{\rho}_x \equiv n_x/\Delta\eta$ and $\bar{\rho}_0 = \bar{\rho}_s + \bar{\rho}_h$. The straight line at right represents the relation $\bar{\rho}_h \approx \alpha\bar{\rho}_s^2$ (as first reported in Ref. [9]) with $\alpha \approx 0.013$ for 5 TeV N-N collisions [6, 23]. It is notable that (a) the lowest four of seven p -Pb n_{ch} classes are effectively equivalent to single peripheral p -N collisions and (b) for higher n_{ch} classes p -Pb centrality *does* increase significantly but jet production (measured by $\bar{\rho}_h/\bar{\rho}_s$) increases less rapidly.

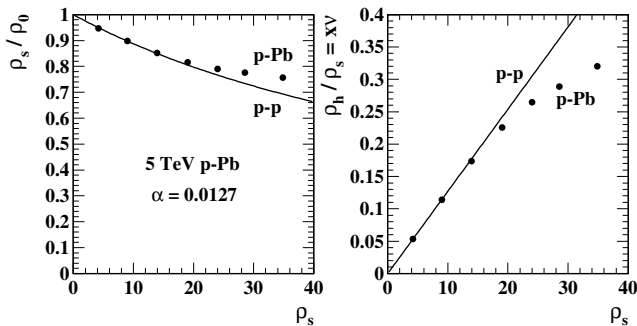


FIG. 7: Soft fraction $\bar{\rho}_s/\bar{\rho}_0$ (left) and hard/soft ratio $\bar{\rho}_h/\bar{\rho}_s \equiv x(n_s)\nu(n_s)$ (right) vs charge-density soft component $\bar{\rho}_s$. The straight line at right represents the relation $\bar{\rho}_h \approx \alpha\bar{\rho}_s^2$ (with $\alpha = 0.013$) that is observed for single N-N collisions [9].

The comparison of TCM and BW spectrum variation with centrality in the previous subsection, while model-independent, is not quantitative and is therefore not conclusive. One can alternatively compare yields at low and high p_t for data (via variable TCM) and the BW model.

Figure 8 compares yields within p_t intervals for $p_t < 0.15$ GeV/c (low) to those for $p_t > 5$ GeV/c (high). The solid points are derived from data extrapolations defined by the *variable* TCM (which represents PID spectrum data accurately as established in Ref. [7]). A reference high-vs-low trend may be derived from the *fixed* PID

TCM from Ref. [6] as follows. Since [6]

$$\begin{aligned} \bar{\rho}_{si} &\approx z_{si}(n_s)\bar{\rho}_s \quad \text{and} \\ \bar{\rho}_{hi} &\approx z_{hi}(n_s)\bar{\rho}_h \approx \tilde{z}_i x(n_s)\nu(n_s)\bar{\rho}_{si} \end{aligned} \quad (6)$$

for hadron species i then high $\approx \tilde{z}_i x(n_s)\nu(n_s) \times$ low assuming fixed TCM model functions (solid curves). Values for $x(n_s)$ and $\nu(n_s)$ are taken from Table I and for ratios \tilde{z}_i are derived from Tables IV and V of Ref. [6]. Note that for those tables z_{si} are determined near 0.15 GeV/c ($y_t \approx 1$) while z_{hi} are obtained near 1 GeV/c ($y_t \approx 2.7$).

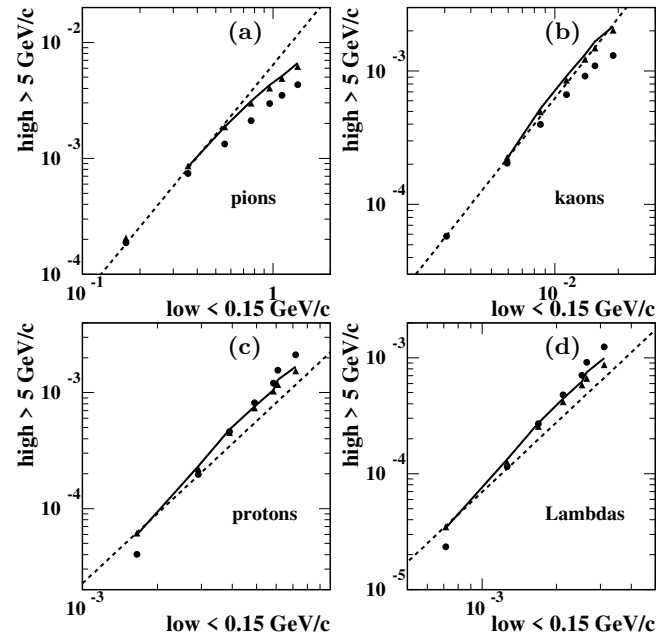


FIG. 8: High vs low spectrum-integral trends (solid dots) for PID data spectra from 5 TeV p -Pb collisions and for (a) pions, (b) neutral kaons, (c) corrected protons, (d) Lambdas. The y_t integrals have the form $(1/2\pi)dn_{ch}/dy_z$. The dashed lines represent high \propto low² reference trends (expected for N-N collisions). The solid triangles are $x\nu \times$ low trends. The solid curves are $\tilde{z}_i x\nu \times$ low trends. Refer to text for further details.

The solid dots represent accurate variable-TCM representations of data spectra integrated over stated p_t intervals. The dashed lines are high \approx low² $\rightarrow x(n_s) \times$ low (reference trends) that would be expected for single peripheral p -N collisions and fixed TCM model functions. The triangles are $x(n_s)\nu(n_s) \times$ low scaled to agree with the p -N (dashed) trend for peripheral collisions. The relation of triangles to dashed lines for pions may be compare with Fig. 7 (right). The solid curves are $\tilde{z}_i x(n_s)\nu(n_s) \times$ low scaled to agree with dashed trends for peripheral collisions again assuming fixed TCM model functions.

Deviations of data trends (solid dots) from $\tilde{z}_i x(n_s)\nu(n_s) \times$ low trends (solid curves) indicate the effect of hard-component model variations with n_{ch} as reported in Sec. III of Ref. [7]. Meson trends fall well below fixed-TCM trends because meson hard components above the mode are transported to lower y_t with increasing p -Pb n_{ch} . While baryon hard components

also vary substantially with increasing n_{ch} (modes transported to *higher* y_t) the variation is mainly below the mode. Baryon solid-dot and solid-curve high vs low trends in panels (c,d) are thus different but much closer.

Those result rely on the TCM to provide accurate descriptions of *absolute* data yields and spectra. As typically utilized, the BW model is not expected to predict absolute yields: “...the normalization of the spectrum...we will always adjust for a best fit to the data...” [1]. However, spectrum high/low *ratios* can be compared between TCM and BW models.

Figure 9 (left) shows high/low (hi/lo) ratios derived from integrals of BW model spectra integrated over $p_t < 0.15$ GeV/c (low) and $p_t > 4$ GeV/c (high) for four hadron species. The lower limit for “high” is reduced compared to the 5 GeV/c limit in Fig. 8 to accommodate the restricted y_t range of the BW model spectra.

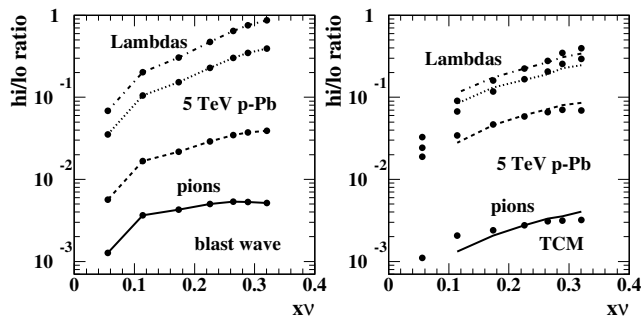


FIG. 9: Left: High/low (hi/lo) ratios derived from integrals of BW model spectra integrated over $p_t < 0.15$ GeV/c (low) and $p_t > 4$ GeV/c (high) for four hadron species. Right: High/low ratios for data represented by the variable TCM. The lower limit for the “high” integral is 4 GeV/c to match the left panel. The curves represent the $\tilde{z}_i x(n_s) \nu(n_s)$ trend expected for fixed spectrum hard components. Note the systematic difference between mesons and baryons as found in Ref. [7].

Figure 9 (right) shows high/low ratios for data (points) represented by the variable TCM. The lower limit for “high” is here 4 GeV/c to match the left panel. The curves are equivalent to solid curves in Fig. 8 representing the $\tilde{z}_i x(n_s) \nu(n_s)$ trend expected for fixed spectrum hard components. The curves are scaled vertically to pass through data points corresponding to event class $n = 4$.

While there is some similarity in the general shapes of BW and data high/low n_{ch} trends, there are large differences in mean values which are due in part to the very different p_t intervals imposed on BW model fits. BW ratios for baryons are a factor 3-4 greater than those for data/TCM. The BW fit interval for baryons is confined to higher p_t and extends well beyond hard-component modes. In contrast, the BW ratio trend for neutral kaons falls significantly below that for data/TCM, and the fit interval extends on p_t from just above the hard-component mode down to zero. The BW ratios for pions are comparable to those for data/TCM, but the p_t fit interval is negligible in comparison to the other cases.

C. Differential spectrum curvatures

While comparisons of high/low ratios as above do provide some quantitative information on spectrum structure they are still not definitive. A more-differential approach is called for. One possibility is logarithmic derivatives. In Ref. [7] Sec. IV E a logarithmic derivative was applied to investigate conjectures in Ref. [4] concerning power-law dependences of integrated p_t intervals on charge density $\bar{\rho}_0$. It was demonstrated there that the approximate power-law trends on $\bar{\rho}_0$ of baryon/meson spectrum ratios resulted from transport of peaked spectrum hard components (for baryons) to higher y_t with increasing n_{ch} , the trends corresponding quantitatively to the Gaussian (+ exponential tail) shapes on y_t of spectrum hard components. In the present context direct analysis of y_t spectra via logarithmic derivative provides the required information.

The logarithmic derivative applied to spectra $\bar{\rho}_0(y_t)$ can be illustrated using the TCM hard-component model [i.e. $\bar{\rho}_0(y_t) \rightarrow \hat{H}_0(y_t)$, see Ref. [7] Eq. (8)]:

$$\begin{aligned} -\frac{d \ln[\bar{\rho}_0(y_t)]}{dy_t} &\rightarrow \frac{y_t - \bar{y}_t}{\sigma_{y_t}^2} \quad \text{near the mode} \\ &\approx q \quad \text{well above the mode.} \end{aligned} \quad (7)$$

The second derivative leads to

$$\begin{aligned} -\frac{d^2 \ln[\bar{\rho}_0(y_t)]}{dy_t^2} &\rightarrow 1/\sigma_{y_t}^2 \quad \text{near the mode} \\ &\approx 0 \quad \text{well above the mode} \end{aligned} \quad (8)$$

The second derivative functions as a measure of *local curvature* or rate of change of local slope of a spectrum.

p -Pb spectra can be characterized in general as follows (based on TCM structure): At low p_t spectra vary as $\hat{S}_0(m_t)$ – approximately as a Boltzmann exponential on m_{ti} with $m_{ti} \rightarrow m_i \cosh(y_{ti})$ for hadron species i . At high p_t spectra approximate a power law on $p_t \sim p_t^n$ (with $p_t \sim m_0 \sinh(y_t)$) or exponential on y_t . Based on those characteristics one expects for Eq. (8)

$$\begin{aligned} -\frac{d^2 \ln[\bar{\rho}_0(y_t)]}{dy_t^2} &\sim \cosh(y_t) \quad \text{at low } p_t \\ &\sim 0 \quad \text{at high } p_t. \end{aligned} \quad (9)$$

Note that $\hat{S}_0(y_t)$ (a Lévy distribution on m_t) itself goes to a power law on m_t at higher y_t . Its logarithmic second derivative should thus also fall to zero at higher y_t .

Figure 10 (left) shows Eq. (8) (left side) applied to neutral kaon spectra from 5 TeV p -Pb collisions as represented by the variable TCM. The kaon data are preferred because of the large y_t acceptance. The line styles proceeding down from most-central are solid, dashed, dotted and dash-dotted followed by solid for the remainder. The trends at low y_t correspond to $\cosh(y_t)$ and at high y_t drop to zero as anticipated by Eq. (9). The hatched band

corresponds to $1/\sigma_{y_t}^2$ for neutral kaons (see Table II). The trend expected for data hard components alone is constant (within the hatched band) terminating near $y_t = 4$ (where the hard component transitions from Gaussian to exponential) dropping toward zero above that point. Variation between $y_t = 2$ and 4 corresponds to relative contributions of soft and hard components at a given y_t varying with p -Pb centrality (\sim product w).

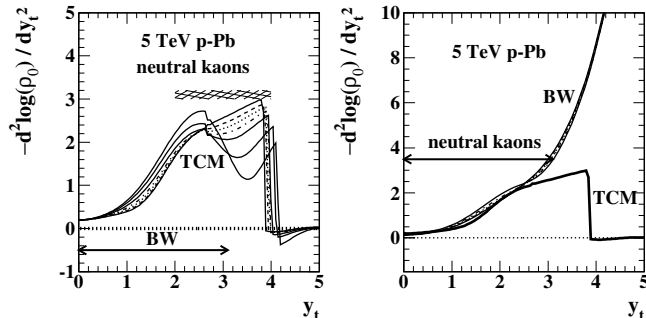


FIG. 10: Left: Logarithmic second derivative Eq. (8) applied to variable TCM spectra accurately representing data for neutral kaons. Line styles proceed down from most-central as solid, dashed, dotted, dash-dotted. The hatched band is limiting case $1/\sigma_{y_t}^2$ for Eq. (8). Right: Logarithmic second derivative Eq. (8) applied to BW spectra with the same line-style sequence. The bold solid curve is the $n = 1$ most-central curve from the left panel.

Figure 10 (right) shows Eq. (8) (left side) applied to BW spectra (curves of several line styles) as reported in Ref. [4] and as in Fig. 6 (a). The result for the variable TCM representing most-central ($n = 1$) p -Pb data (left panel) is included as a reference. The strong deviation between BW and data/TCM is evident above $y_t = 2.5$ ($p_t \approx 0.8$ GeV/c). Variation of BW model parameters with n_{ch} leads to rather small spectrum shape variations (compared to the left panel) below $y_t = 3$ where χ^2 fits should matter. What follows is a procedure to examine the effect of varying each of three BW parameters in turn.

D. BW model response to individual parameters

Figure 11 (a) shows the effect of varying “kinetic freeze-out” temperature T_{kin} over the values reported in Ref. [4] while holding the other two parameters fixed at their values for middle centrality $n = 4$. The result is relatively little variation of BW spectrum shapes.

Figure 11 (b) shows the effect of varying mean radial speed $\bar{\beta}_t$ over its reported values while holding the other two parameters fixed. The result is large variation of curvatures, spectra being shifted strongly to *higher* y_t with increasing centrality across the entire y_t interval.

Figure 11 (c) shows the effect of varying flow-profile parameter n over its reported values (per Table III) while holding the other two parameters fixed. The result is moderate shift of spectra to *lower* y_t with increasing cen-

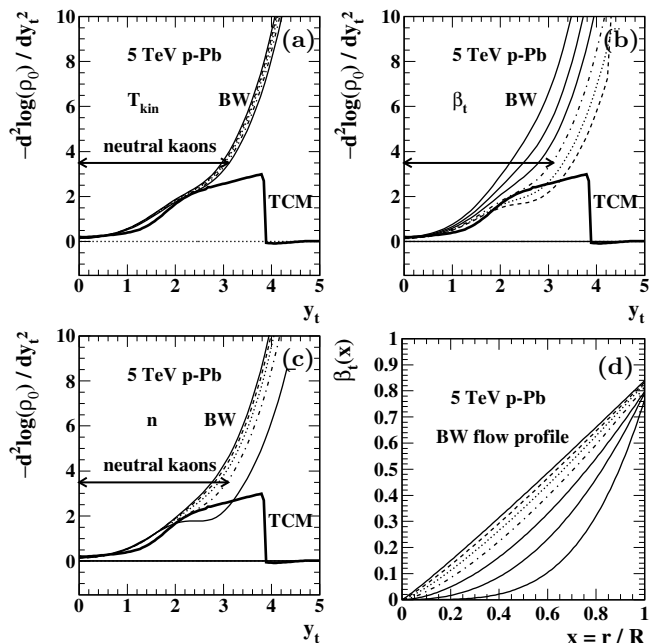


FIG. 11: BW second derivatives with only one parameter varying: (a) T_{kin} varies, (b) $\bar{\beta}_t$ varies, (c) profile parameter n varies. In each case other BW parameters are maintained at centrality $n = 4$ values and the TCM reference for $n = 1$ is included. (d) BW $\beta_t(r)$ profiles for seven p -Pb centralities.

trality, but only above $y_t = 2$. Figure 11 (d) shows the effect of varying parameter n on the “flow profile” or variation of radial speed $\beta_t(x)$ with fractional radius $x = r/R$.

Based on Fig. 11 (a) and Z-scores in the next section the BW model as applied to neutral kaons is not relevant above $y_t \approx 2.8$ ($p_t \approx 1.15$ GeV/c). Below that point T_{kin} does not significantly affect the model compared to the other two BW parameters (acts mainly as an overall scale factor that is seen as not relevant). $\bar{\beta}_t$ affects the model over a broad interval but n is controlling only above $y_t = 1.8$ ($p_t \approx 0.4$ GeV/c), and the two parameters produce strongly opposing variations in spectrum shape. In effect, the BW model as applied to neutral kaons is a two-parameter model function that attempts to describe data over a limited p_t interval. Based on the above results physical interpretation of model parameters *directly* via comparisons with data trends seems problematic.

Figure 12 (left) shows the effect of turning off radial flow ($\bar{\beta}_t = 0$). The shape change corresponds to faster fall-off with decreasing T_{kin} value (and *increasing* p -Pb centrality). The bold dotted curve is the Boltzmann (exponential on m_t) limit of $\hat{S}_0(y_t)$ (i.e. if Lévy exponent $n \rightarrow \infty$) with $T = 145$ MeV. BW model spectra approach that limit for central p -Pb collisions and $T_{kin} \approx 145$ MeV.

Figure 12 (right) shows the effect of holding temperature T_{kin} fixed at 145 MeV while the other two parameters remain consistent with Table III. The BW model fitted to the most-peripheral p -Pb data (with $\bar{\beta}_t \approx 0.25$) corresponds closely to TCM model $\hat{S}_0(y_t)$ (bold dashed).

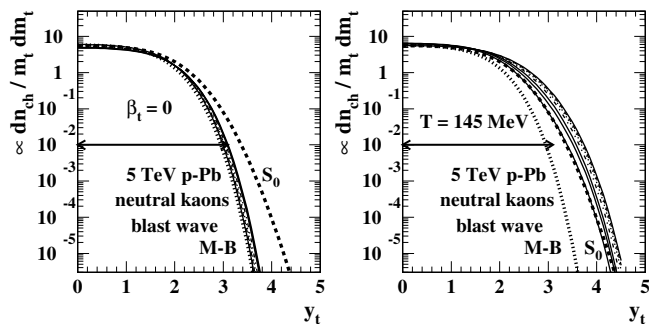


FIG. 12: Left: BW model spectra with $\bar{\beta}_t = 0$ (various line styles). $\hat{S}_0(y_t)$ (bold dashed) corresponds to $T_i = 200$ MeV for kaons. The reference Boltzmann distribution (bold dotted) corresponds to $T = 145$ MeV. Right: BW model spectra with fixed $T_{kin} = 145$ MeV (= TCM T value for unidentified hadrons) with $\bar{\beta}_t$ and n varying as in Table III.

Note that $\hat{S}_0(y_t)$ for the TCM (bold dashed) in the left panel is *defined* to match data spectra as $n_{ch} \rightarrow 0$. As such it has no jet contribution and represents *zero particle density*. The BW model with no jet component and zero flow contribution should have the best opportunity to describe spectrum data there *given BW model assumptions*. But the BW model strongly deviates from $\hat{S}_0(y_t)$ above $y_t = 2$ ($p_t \approx 0.5$ GeV/c). BW curves with $\bar{\beta}_t = 0$ and $T_{kin} \approx 145$ MeV (central p -Pb in Table III) instead closely approximate a Boltzmann exponential (bold dotted) on transverse mass m_t with slope parameter $T = 145$ MeV scaled to coincide with $\hat{S}_0(y_t)$ at low y_t .

The power-law tail on $\hat{S}_0(y_t)$ (as a Lévy distribution [24]) can be interpreted to represent inhomogeneity of the emitting system, i.e. the Lévy model parameter n can be expressed in the form $1/n \sim \sigma_T^2/\bar{T}^2$ [25]. The inferred width σ_T may be interpreted in terms of incomplete equilibration or in terms of k_t broadening within a longitudinal splitting cascade. The result in the right panel suggests that a substantial part of the $\bar{\beta}_t$ contribution simply accommodates the Lévy shape of soft component $\hat{S}_0(y_t)$ common to all A-B collision systems and has nothing to do with radial flow *per se*. That explains why low- n_{ch} p - p and peripheral A-B collision data require $\bar{\beta}_t \approx 0.25$ [26] for Boltzmann-based BW models.

V. BW vs TCM SPECTRUM FIT QUALITY

This section quantitatively evaluates spectrum fit quality for the BW model compared to the TCM as applied to 5 TeV p -Pb collisions. Three goodness-of-fit measures are compared: (a) Z-scores, (b) χ^2 and (c) data/model spectrum ratios. Fit quality based on statistical errors is compared with that based on systematic errors, both as published with spectrum data in association with Ref. [4].

A. Goodness-of-fit measures

A standard measure of data description or fit quality for a model is the Z-score (for an i^{th} observation) [27]

$$Z_i = \frac{O_i - M_i}{\sigma_i}, \quad (10)$$

where O_i is an observation (datum), M_i is a model prediction and σ_i is the uncertainty (“error”) for the corresponding observation. In some presentations $M_i \rightarrow E_i$ (expectation) and $\sigma_i \rightarrow \sqrt{E_i}$ (assuming Poisson statistics for O_i). For an acceptable model one expects Z_i to have an r.m.s. value near 1. The χ^2 statistic is simply related:

$$\chi^2 = \sum_{i=1}^N Z_i^2 \quad (11)$$

for N data points. An acceptable model should yield $\chi^2 \sim \nu = N - D$ where D is the number of degrees of freedom of the model (e.g. number of model parameters).

There is a tendency to evaluate model quality in terms of data/model *ratios* – e.g. Fig. 7 of Ref. [4]. The relation between data/model ratios and Z-scores is

$$\frac{\text{data}}{\text{model}} - 1 \approx \text{Z-score} \times \frac{\text{error}}{\text{data}}, \quad (12)$$

with error/model (exact) \rightarrow error/data (approximate). The error/data ratio may vary by orders of magnitude between different particle types and collision systems, and even across y_t intervals (see Figs. 17 and 18). Whereas the correct test of model validity is the relation of Z-scores to 1 (or χ^2 to ν) the interpretation of data/model ratios relative to 1 is problematic and typically quite misleading. The error/data ratios on the right are typically $\ll 1$ thereby suppressing, in data/model ratios on the left, what may be very significant data-model deviations.

B. Fit quality based on statistical uncertainties

Figures 13 and 14 (a,c) compare BW model fits (dashed) to p -Pb spectrum data (solid). The spectrum data are scaled as shown in the y -axis labels and as reported in Refs. [6, 7]. The BW curves correspond to the fitted parameters in Table III and are scaled to best match the data, consistent with the fitting procedure.

Figures 13 and 14 (b,d) show Z-scores for BW model vs spectrum data using statistical uncertainties that accompany the published data. It is evident that even within y_t intervals chosen to produce an acceptable fit [4] the Z-scores are consistently substantially greater than 1. Results for BW fits can be compared with results from a TCM analysis of the same data reported in Refs. [6, 7].

Figures 15 and 16 compare data/TCM ratios (left panels) to Z-scores (right panels), for mesons (pions and kaons) in Fig. 15 and for baryons (protons and Lambdas) in Fig. 16. Based solely on data/model ratios it would

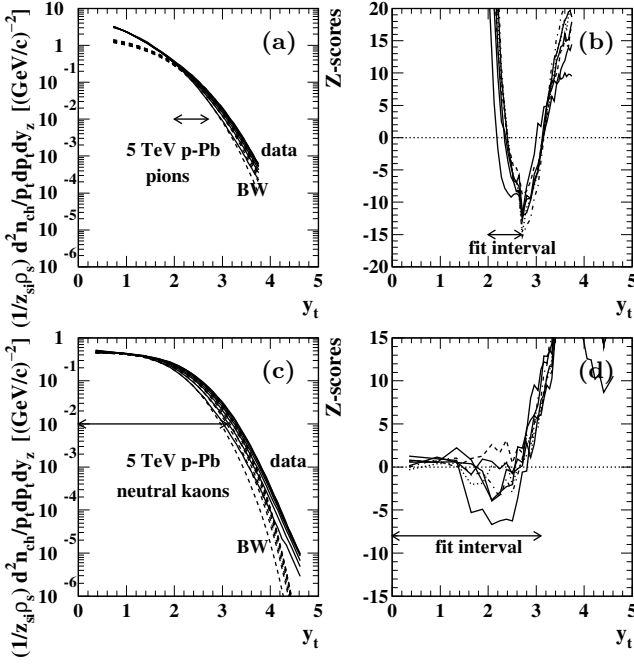


FIG. 13: Data p_t spectra (solid) for pions (a) and neutral kaons (c) and corresponding BW model curves (dashed). Data spectra are rescaled to quantity $X_i(y_t)$ as defined in Eq. (3). BW curves are scaled to match the data within fit intervals (arrows). Panels (b,d) show corresponding Z-scores based on *statistical* errors published with the spectrum data.

seem that the TCM description for pion data is much better than that for Lambda data. Yet a comparison of corresponding Z-scores shows that the data descriptions are actually of comparable quality. While Z-scores within some y_t intervals are consistent with statistical deviations (i.e. r.m.s. consistent with 1) prominent localized excursions are apparent – for instance y_t near 2 for pions and y_t within 2-3 for protons. Given that the significant data-TCM deviations are consistent across p -Pb n_{ch} classes and highly localized on y_t it is unlikely that the deviations result from model issues. It is reasonable to conjecture that such structures are inevitable within the complex procedure of processing particle data. These results suggest that the TCM describes p -Pb PID spectrum data within statistical uncertainties except for local anomalies that may be due to detector effects.

C. Fit quality based on systematic uncertainties

The BW-fit χ^2/ndf values appearing in Table III, as reported in Ref. [4], are notable for two reasons: they are (a) consistently *low* compared to the expected r.m.s. value ≈ 1 for acceptable fits and (b) apparently at odds with the Z-scores shown in Figs. 13 and 14 that are consistent with χ^2/ndf values substantially greater than 10. Those results suggest that χ^2/ndf values reported in Ref. [4] were obtained assuming *systematic*

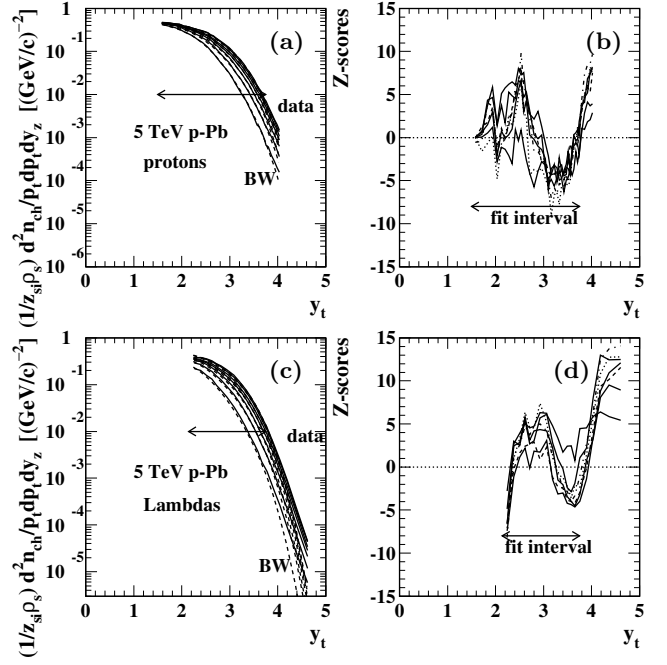


FIG. 14: Data p_t spectra for protons (a) and Lambdas (c) (solid) and corresponding BW model curves (dashed). Data spectra are rescaled to quantity $X_i(y_t)$ as defined in Eq. (3). BW curves are scaled to match the data within fit intervals (arrows). Panels (b,d) show corresponding Z-scores based on *statistical* errors published with the spectrum data.

rather than statistical uncertainties σ_i in Eq. (10).

Figures 17 and 18 (a,c) show BW-fit Z-scores recalculated using systematic errors included with published p -Pb spectra from Ref. [4]. Vertical scales are the same as those in Figs. 13 and 14 (a,c) for comparison. Those results suggest that systematic uncertainties were in fact used to calculate χ^2/ndf values appearing in Table III.

Figures 17 and 18 (b,d) compare published p -Pb systematic uncertainties (dashed) with statistical uncertainties (solid) in ratio to corresponding spectrum data values. Systematic uncertainties are approximately constant on y_t with magnitudes 5-10% of data values. The numbers are consistent with *total* systematic uncertainties presented in Tables 3 and 4 of Ref. [4]. The systematic uncertainties tend to exceed statistical uncertainties by a factor five or more, especially within fit intervals employed for BW fits, implying that reported χ^2/ndf values are at least a factor 25 less than what would be obtained using statistical uncertainties. That description responds to items (a) and (b) at the beginning of this subsection.

Appropriate uncertainty estimates are of central importance for realistic assessment of model quality. The most basic estimate (where data result from counting discrete elements – e.g. particles) is the statistical uncertainty corresponding to Poisson statistics. Corresponding Z-scores then show all *statistically significant* data-model deviations no matter what their origin. Various sources of systematic uncertainty, whether correlated

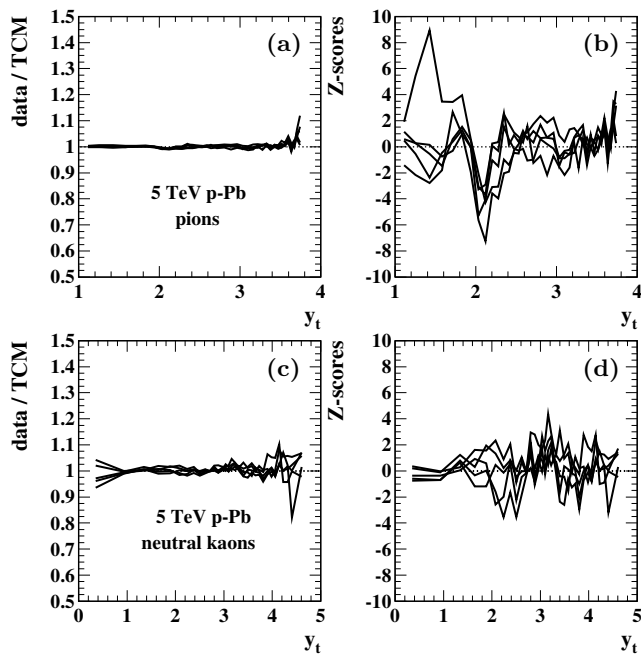


FIG. 15: Left: Data/TCM spectrum ratios for pions (a) and neutral kaons (c). Right: Z-scores for pions (b) and neutral kaons (d). The model is the *variable* TCM defined in Ref. [7].

with collision event class (n_{ch}) or particle properties (y_t , hadron species) or not, may be relevant to correct assessment of model quality but should be considered only relative to Z-scores based on statistical uncertainties.

More generally the χ^2 statistic is not very effective for model testing. χ^2 is intended to measure a significant difference between model and data but contains much less information than the differential Z-scores it represents as in Eq. (11). Z-scores based on statistical errors clearly show not only what data-model differences are statistically significant but also how such deviations are correlated, e.g. across y_t bins and n_{ch} classes. In comparing two models the one with the greater χ^2 may even be preferred because of the detailed structure of Z-scores.

VI. BLAST WAVE MODEL EVOLUTION

In order to interpret BW model fit results it is useful to review early theoretical developments that led to the current general form applied to ultrarelativistic A-B collisions and some significant variations in the structure of the model over several decades.

A. Early BW model development

The blast-wave model arguably has its origins in the collision theories of Landau (1950s, e.g. Ref. [28]) and Hagedorn (1960s, e.g. Ref. [29]). Hadron production is based in the first case on hydrodynamic evolution

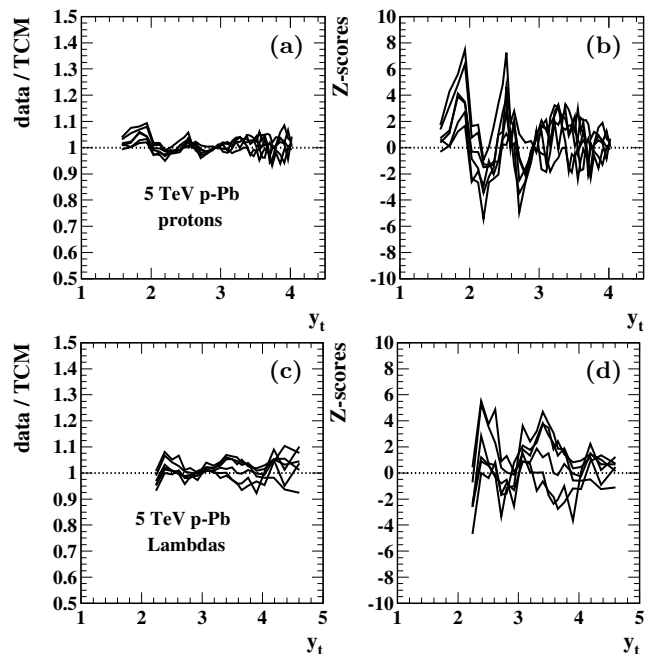


FIG. 16: Left: Data/TCM spectrum ratios for protons (a) and Lambdas (c). Right: Z-scores for protons (b) and Lambdas (d). The model is the *variable* TCM defined in Ref. [7].

of a hadronic fluid and in the second case on emission from rapidly-moving “fireballs.” In either case “collectivity” – collective motion of a continuous hadronic fluid or discrete collection of objects (fireballs) in configuration space – is a central feature. Detected hadrons that emerge are thereby *correlated* in momentum space, such correlations interpreted to indicate a form of collectivity.

The correct relation between the measured particle momentum distribution in the center-of-momentum (CM) or laboratory (lab, for symmetric colliders) frame and the hadron emission distribution in the local, co-moving or boost frame was determined by Cooper and Frye [5] as

$$E \frac{d^3 N}{dp^3} = \frac{d^3 N}{m_t dm_t dy_z d\phi_p} = \int_{\sigma} f(xpu) p^\mu d^3 \sigma_\mu, \quad (13)$$

where $u(x)$ is the velocity field of an emitting fluid in the lab frame, p^μ is the particle four-momentum measured in the lab frame, σ is the “freezeout” hypersurface (\sim transition from small to large mean free path), and $d^3 \sigma_\mu$ is a differential volume four-vector. A limiting case for $f(xpu)$ in the local or boost frame is isotropic emission, according to Bose or Fermi statistics or (as an approximation) the Boltzmann distribution. That formalism was employed to describe spherical expansion within nucleus-nucleus collisions in Ref. [31] wherein the term “blast wave” was introduced in connection with A-B collisions. More complex expansion geometries (i.e. *nucleon* flows) were encountered within the Bevalac program [32].

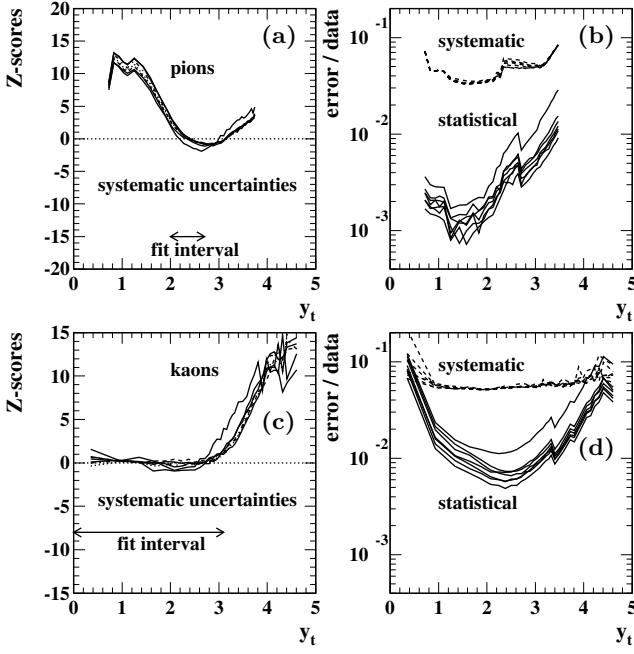


FIG. 17: BW model Z-scores for pions (a) and neutral kaons (c) based on *systematic* uncertainties or errors published with spectrum data. Panels (b,d) show error/data ratios for statistical errors (solid) and systematic errors (dashed).

B. BW model for ultrarelativistic A-B collisions

For the Bevalac and alternating gradient synchrotron (AGS) nucleus-nucleus programs, where the collision energy per nucleon is of order the nucleon mass-energy, fractional deviations from spherical expansion (e.g. squeeze-out, side-splash) were measured via the sphericity tensor or related measures [33, 34]. For A-B collisions at the super proton synchrotron (SPS), RHIC or LHC, collision energies are much greater than the nucleon mass-energy. As a consequence the velocity field represented by $u(x)$ above is highly asymmetric – strongly elongated along the collision axis. Reference [1] reported a version of Eq. (13) adapted to that context and applied to SPS S-S collisions at $\sqrt{s_{NN}} \approx 19$ GeV. It is useful to examine details of the derivation and accompanying arguments.

It is assumed that within a local (co-moving or boost) frame hadron emission is locally thermal and isotropic (i.e. within a *transparent* environment): “...the invariant distribution function [in the CM or lab frame]...we assume to be an isotropic thermal distribution boosted by the local fluid velocity u^μ , and we approximate the respective Bose and Fermi distributions by the Boltzmann distribution.” Equation (13) is modified by

$$f(xp) \rightarrow [g (2\pi)^3] \exp[-(u^\nu p_\nu - \mu)/T], \quad (14)$$

and potential μ is omitted below (see comment below on “normalization”). Configuration space is represented by

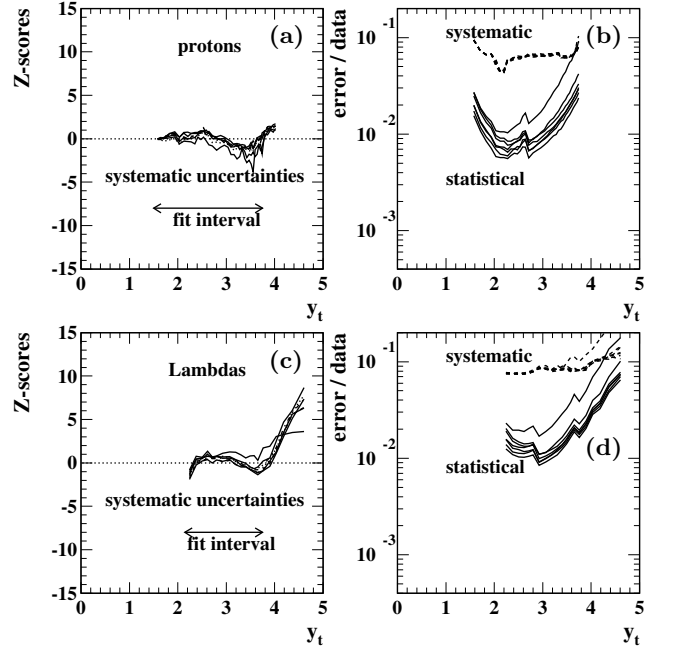


FIG. 18: BW model Z-scores for protons (a) and Lambdas (c) based on *systematic* uncertainties or errors published with spectrum data. Panels (b,d) show error/data ratios for statistical errors (solid) and systematic errors (dashed).

cylindrical coordinates with a hypersurface defined by

$$\begin{aligned} \sigma_\mu &= [t(\eta_s), r\hat{e}(\phi_x), z(\eta_s)] \\ &= [\tau \cosh(\eta_s), r\hat{e}(\phi_x), \tau \sinh(\eta_s)] \end{aligned} \quad (15)$$

with $\zeta \rightarrow \eta_s$ and

$$\begin{aligned} d^3\sigma_\mu &= \left[\frac{\partial z}{\partial \eta_s}, 0, 0, \frac{\partial t}{\partial \eta_s} \right] d\eta_s d\phi_x \\ &\rightarrow \tau [\cosh(\eta_s), 0, 0, \sinh(\eta_s)] d\eta_s d\phi_x. \end{aligned} \quad (16)$$

Space-time rapidity is $\eta_s = (1/2) \ln[(t+z)/(t-z)] = \ln[(t+z)/\tau]$. Quantities u_μ and p_μ are as defined in Eqs. (A5) and (A6). Whereas Ref. [1] invokes “flow angles” ρ and η , equivalent quantities are presented here by η_t and η_z respectively. The conventional assumption $\eta_z \rightarrow \eta_s$ is consistent with Bjorken expansion.

Given those definitions Eq. (13) then becomes

$$\begin{aligned} \frac{d^3N}{m_t dm_t dy_z d\phi_p} &= \frac{g}{(2\pi)^3} m_t \\ &\times \int_{-H_s}^{H_s} d\eta_s \left[\cosh(y_z) \frac{\partial z}{\partial \eta_s} - \sinh(y_z) \frac{\partial t}{\partial \eta_s} \right] \\ &\times \int_0^R dr \exp\{-m_t \cosh[\eta_t(r)] \cosh(y_z - \eta_z)/T\} \\ &\times \int_0^{2\pi} d\phi_x \exp\{p_t \sinh[\eta_t(r)] \cos(\phi_x - \phi_p)/T\}, \end{aligned} \quad (17)$$

where $\eta_s \in [-H_s, H_s]$ delimits the particle source. The

quantity in square brackets then simplifies to

$$\cosh(y_z) \frac{\partial z}{\partial \eta_s} - \sinh(y_z) \frac{\partial t}{\partial \eta_s} \rightarrow \tau \cosh(y_z - \eta_s). \quad (18)$$

The integral over ϕ_x reduces to $2\pi I_0[p_t \sinh(\eta_t)/T]$. Using Eq. (18) and integrating both sides over y_z leads to integrand $K_1[m_t \cosh(\eta_t)/T]$ in the third line. “We obtain the transverse mass spectrum $d^4m_T dm_T$ by integrating over rapidity $[y_z]$ using the modified Bessel function $K_1\dots$ ” The integral over η_s then simply leads to factor $2Z_t \rightarrow 2H_s$ consistent with the interval over space-time rapidity $\zeta \rightarrow \eta_s$ assumed in Eq. (14) of Ref. [1]. The result is Eq. (5) above except $\rho \rightarrow \eta_t = \tanh^{-1}(\beta_t)$, with $\beta_t(r) = \beta_s(\not{r}R)^n$. That expression is used by Ref. [4] to obtain the BW model fits summarized in Sec. III.

As noted, the absolute scale of the BW model in relation to spectrum data is not seen as significant (in contrast to the TCM). Reference [1] concludes: “...we have shown that a thermal model is perfectly possible for S+S collisions despite (or because of?) the similarity of S+S and pp spectra. The data force us to include resonance decays and longitudinal flow while they make no decisive statement about the existence of transverse flow.”

C. Alternative BW model applications

It is informative to examine some alternative routes to BW model functions and their applications to a variety of collision data. The examples below relate to the experimental programs at the SPS, RHIC and LHC. Further details on BW model derivations and applications are provided in App. A.

1. Tomásik, Wiedemann and Heinz [35]

The study in Ref. [35] combines BW spectrum analysis of single-particle spectra and Bose-Einstein correlation (BEC) analysis of two-particle correlations to infer space-time properties of the particle source (emission region, freezeout state). The models (BW + BEC) were applied to NA49 data from 158A GeV Pb-Pb collisions. The particle source is modeled by an “emission function” $S(xp)d^4x$ that includes the factor $p^\mu d^3\sigma_\mu$ from Eq. (13) plus densities on r , η_s and τ that explicitly define the integrated space-time (source) volume.

Combining Eqs. (3.1) and (3.10) from Ref. [35]

$$\begin{aligned} E \frac{d^3N}{dp^3} &= \int S(xp)d^4x \quad (19) \\ &= \frac{1}{(2\pi)^3} \int d\eta_s dd\phi_x G(r)H(\eta_s)T(\tau) \\ &\quad \times m_t \tau \cosh(y_z - \eta_s) \exp[-(u^\nu p_\nu - \mu)/T], \end{aligned}$$

where $H(\eta_s)$ and $T(\tau)$ are Gaussians on η_s and τ respectively, the latter normalized to unity. $p_\mu =$

$[m_t \cosh(y_z), p_t, 0, m_t \sinh(y_z)]$. $G(r)$ is modeled as a Gaussian or square (flat) distribution on r . In contrast, Ref. [1] implicitly assumes flat distributions on r and η_s and a delta function on τ . Velocity field $u(x)$ is initially defined in terms of longitudinal $\eta_l \rightarrow \eta_z$ and transverse η_t “expansion rapidities” (boosts) and $u(x)$ is then as in Eq. (A5). η_l is then identified with space-time rapidity $\eta \rightarrow \eta_s$ (i.e. Bjorken expansion). In Ref. [1] transverse speed is parametrized by $\beta_t(r) = \beta_s(\not{r}R)^n$ but Ref. [35] expresses transverse *boost* as $\eta_t(r) = \eta_f(\not{r}r_{rms})$.

2. Florkowski and Broniowski [36]

Reference [36] briefly summarizes the history of the BW model and then presents an alternative route to the model as it appears in Eq. (5). Symbols used in Ref. [36] are related to the standard set employed in this study.

Space-time rapidity is $\alpha_{||} \rightarrow \eta_s$ (what correlates t and z given proper time τ). ζ is a parameter that correlates proper time τ and radius $\rho \rightarrow r$. That system is assumed boost invariant over all η_s in contrast to [1]. Thus, instead of $[t(\zeta), z(\zeta)]$ with $\zeta \rightarrow \eta_s$ space-time rapidity there is $[\tau(\zeta), r(\zeta)]$ with $\zeta \in [0, 1]$ simply a correlation parameter. $\sigma_\mu(x)$ is formally as in the second line of Eq. (15), but the differential volume element $d^3\sigma_\mu$ (with $\rho \rightarrow r$) is

$$\left[\frac{dr}{d\zeta} \cosh(\eta_s), \frac{d\tau}{d\zeta} \hat{e}(\phi_x), \frac{dr}{d\zeta} \sinh(\eta_s) \right] d\zeta \tau d\eta_s d\phi_x. \quad (20)$$

$u(x) = \cosh(\eta_t)[\cosh(\eta_z), \tanh(\eta_t)\hat{e}(\phi_x), \sinh(\eta_z)]$ is the velocity field (corrected from Ref. [36]) with $\alpha_\perp \rightarrow \eta_t$ and in this case $\alpha_{||} \rightarrow \eta_z$. Longitudinal flow is represented by $v_z \rightarrow \beta_z = \tanh(\eta_z)$, and transverse flow by $\beta_t(\zeta) = \tanh[\eta_t(\zeta)]$. β_t is correlated with τ and r by parameter ζ as alternative to explicit $\beta_t(r) = \beta_s(\not{r}R)^n$ in Ref. [1]. p_μ and $u^\mu p_\mu$ are as in Eqs. (A6) and (A7).

The transverse component $d\tau/d\zeta$ in Eq. (20) would introduce additional complexity compared to Eq. (17) and is assumed zero in Ref. [36] “to achieve the simplest possible form of the model.” $d^3\sigma_\mu$ then has the form of Eq. (16) (second line) except $d\zeta \rho(\zeta) d\rho/d\zeta \rightarrow dr$. Equation (28) of Ref. [36] corresponds to Eq. (17) with $g \rightarrow 1$, but its Eq. (29) assumes that $\alpha_\perp(\zeta) \rightarrow \eta_t(\zeta)$ is constant.

3. Rath, Khuntia, Sahoo and Cleymans [22]

The BW model invoked in Ref. [22] is nominally that of Ref. [1] but differs substantially as follows. The differential volume element is given as

$$d^3\sigma_\mu = \tau [\cosh(\eta_s), 0, 0, [-] \sinh(\eta_s)] d\eta_s dd\phi_x \quad (21)$$

but the bracketed minus sign is incorrect – compare Eq. (16) (second line). Quantities u_μ and p_μ are as defined in Eqs. (A5) and (A6). Quantity $\eta \rightarrow \eta_s$ is space-time rapidity. It is notable that “Bjorken correlation in rapidity” is interpreted as $(y = \eta) \rightarrow (y_z = \eta_s)$. In that

case the expression in Eq. (18) above goes to τ and the integration over η_s in Eq. (17) is trivial. Function $K_1(x)$ could not arise based on that assumption. It would be replaced by an exponential with the same arguments.

Explicitly, η_s is space-time rapidity parameterizing $\sigma_\mu(x)$ and is usually assumed equivalent to longitudinal boost η_z in velocity field $u_\mu(x)$ (Bjorken expansion), both of those being flows in configuration space. The assumption $y_z = \eta_s$ equates longitudinal rapidity y_z of detected particles in momentum space with space-time rapidity or boost of a particle source in configuration space. Equation (14) of Ref. [22] appears to be missing a combined factor $p_t m_t$ or m_t^2 compared to Eq. (17). The analysis is based on taking $n = 1$ for “flow profile” $\beta_t(r) \propto (\not{r}R)^n$.

4. Ray and Jentsch [37]

Reference [37] uses the BW model as formulated in Ref. [35] to study the effect of event-wise fluctuations within A-A collisions and their manifestations in single-particle spectra on transverse rapidity $y_t = \ln[(p_t + m_t)/m_0]$ and on two-particle correlation space (y_{t1}, y_{t2}) . The single-particle distribution in Ref. [37] is derived from Ref. [35] [see Eq. (19) above] but it is assumed that $y \rightarrow y_z \approx 0$. That is a reasonable assumption for data near midrapidity and for the higher energies at the RHIC and LHC in contrast to Ref. [1] relying on integration over y_z to obtain Eq. (5) for description of SPS S-S data at $\sqrt{s_{NN}} \approx 19$ GeV. The expression on the right in Eq. (18) then becomes $\tau \cosh(\eta_s)$ (with $\tau_0 \rightarrow \tau$). In Eq. (17) $\cosh(y_z - \eta_z) \rightarrow \cosh(\eta_z)$ in the exponential.

5. Lao, Liu and Ma [38]

Reference [38] invokes the BW model as reported in Eq. (18) of Ref. [37] to produce its Eq. (1). A “blast-wave model with fluctuations” is attributed to Ref. [35] but the word “fluctuations” does not appear in that document. Reference [37] does describe a BW model with fluctuations but their Eq. (18), adopted from Ref. [35] and the basis for Eq. (1) of Ref. [38], appears before the subject of fluctuations (in $\beta = 1/T$ and in radial boost η_t) is addressed. In Ref. [38] $y \rightarrow y_z$ remains variable whereas $\cosh(y_z - \eta_z) \rightarrow \cosh(y_z) \cosh(\eta_z)$ is assumed. The derivation then proceeds to “single source emission” wherein $\eta_s \rightarrow 0$ and source distribution $H(\eta_s) \rightarrow 1$. The particle source is thereby modeled effectively as a thin disk at $\eta_s = 0$. As a result $K_1[m_t \cosh(\eta_t)/T]$ in Eq. (5) $\rightarrow \exp[-m_t \cosh(y_z) \cosh(\eta_t)/T]$ in Eq. (4) of Ref. [38]. The $\beta_t(r)$ flow-profile parameter $n_0 \rightarrow n$ is held fixed at 2. It is further remarked that “ n_0 is not a sensitive quantity. It does not matter if $n_0 = 1$ or $n_0 = 2$.” But refer to Fig. 11 (c) for the strong effect of parameter n .

Equation (4) of [38] is then applied to a broad array of LHC A-B collision data. The study notes “...one can see that we have used the species-dependent parameters to fit

the spectra... [i.e. BW fits to individual hadron species]. This is not the usual way to use the blast-wave model, which fits various spectra simultaneously. We have examined the simultaneous fit of the model for various spectra and know that narrow and different p_T ranges have to be used for different particles [e.g. Ref. [4]]. We do not think that the simultaneous fitting of various spectra can be better in wide p_T ranges. Instead, we may use the individual fit for different spectra and obtain better fits.”

Even with fits to individual hadron species χ^2/ndf numbers are often much greater than 1. Reference [38] comments that large χ^2/ndf values “...indicates that the fitting was qualitative and approximately acceptable, and the large dispersion between the curve and data exists.” One observation is notable in the context of the present study: “However, the disadvantage of the [BW] model is also obvious. In some cases, one[-]component model cannot fit the data well. In fact, it is only applicable to the low- p_T region, but not to the high- p_T region. This problem is not only a disadvantage in the blast-wave model...but also a disadvantage in all thermal models.”

These examples serve to illustrate several BW issues: Assumptions vary concerning the structure of the flow field and emission volume and how they should be represented. Concerning derivation of a specific BW model function the basic Cooper-Frye context is accepted. However, significant details of derivations vary. Different symbol choices by authors for basic kinematic quantities complicate interpretation. There is also substantial variation concerning BW model application to data: e.g. a common fit to all hadron species as opposed to individual fits to species. There is the question what p_t fit intervals should be used, as determined by what criteria? It is not clear how fits to data might be used to clarify such ambiguities. As a matter of interpretation is there any circumstance in the comparison of model to data wherein the BW model (which version?) might be falsified?

6. Tsallis-BW models [39]

A basic assumption of the BW models above is that any deviation from a *Boltzmann* exponential (say below $m_t \approx 3$ GeV/c) must arise from a moving particle source as in fluid flow [1]. That assumption fails for two reasons: (a) The Boltzmann exponential is an idealization quite unlikely in real situations, especially in relation to parton splitting cascades resulting in heterogeneous systems (parton showers) as hadron sources. (b) The strong contribution from minimum-bias jet fragments (from large-angle-scattered partons) extends down to 0.5 GeV/c with a peak near 1 GeV/c. That system is described accurately by the TCM as demonstrated for 5 TeV p -Pb collisions in Secs. II and V B and Refs. [6–8].

Incorporation of the *Tsallis* spectrum model (q -exponential, Tsallis statistics) as a replacement for the Boltzmann exponential within the BW model formulation [39] is, in effect, an attempt to deal with (a) but relies

on variation of Tsallis model parameters with A-B centrality which is never observed for soft component $\hat{S}_0(m_t)$ of the TCM. As a monolithic spectrum model the Tsallis model has, *in principle*, no capacity to accommodate item (b) above. But model parameters T and q are varied as an attempt to accommodate strong increase of the jet contribution with centrality. Model fits in Ref. [39] are restricted to the range $p_t \in [0.5, 3]$ GeV/c.

The main difference from the Boltzmann BW versions is that $\bar{\beta}_t$ for p - p and peripheral A-B collisions is now consistent with zero as one might expect, since the Tsallis model is a variant of soft-component model $\hat{S}_0(m_t)$ that describes all A-B soft components within statistical uncertainties. Ironically, the *decrease* with increasing centrality of Tsallis parameter $q - 1$ (corresponding to increase of TCM parameter n indicating softening of the $\hat{S}_0(m_t)$ power-law tail) may actually respond in part to “jet quenching.” Although it cautions that “...the physical interpretation of this [Tsallis] statistical model in the context of high energy nuclear collisions remains to be fully understood” Ref. [39] interprets the $q - 1$ trend as “...indicating an evolution from a highly non-equilibrated system in p+p collisions toward an almost thermalized system in central Au+Au.” There is no acknowledgement of a jet contribution to spectra assumed (erroneously) as confined to “high- p_T particles.” The possibility that parameter $\bar{\beta}_t$ and T_{kin} values, as inferred from a BW model effectively falsified by data, may not be physically interpretable is also not considered.

VII. SYSTEMATIC UNCERTAINTIES

Systematic uncertainties for BW model fits to spectra relate to the primary PID spectra, various BW model versions and fit methods and the validity of any BW model version for part or all of the spectrum p_t acceptance.

A. Systematic uncertainties from Ref. [4]

Regarding PID spectra themselves Ref. [4] states that “The main sources of systematic uncertainties for the analysis of charged and neutral particles are summarized in Tables 3 and 4, respectively. The study of systematic uncertainties was repeated for the different multiplicity bins in order to separate the sources of uncertainty which are dependent on multiplicity and uncorrelated across different bins (depicted as shaded boxes in the figures).” From that and other language in the text there are apparently three types of spectrum uncertainties reported: statistical, n_{ch} -dependent and total denoted by solid bars, shaded boxes and unshaded boxes respectively. Captions for Figs. 2, 3, 4 and 5 include “The empty boxes show the total systematic uncertainty; the shaded boxes indicate the contribution uncorrelated across multiplicity bins....”

Spectrum data reported in Ref. [4] apparently include statistical and *total* uncertainties, the latter consistent

with “Total” in Tables 3 and 4 of Ref. [4]. There is no distinction in those tables among systematic errors that are y_t dependent or not and n_{ch} dependent (correlated vs uncorrelated) or not, and there is no estimation of what might contribute to *point-to-point* (on y_t) uncertainties. See Figs. 15 and 16 (right) for statistically-significant systematic *errors* that are correlated across multiplicity n_{ch} bins but uncorrelated (i.e. vary strongly) across y_t bins.

Properly-estimated systematic uncertainties relevant to model descriptions would ideally be consistent with actual data-model discrepancies in the event of a valid model. The results in Figs. 15 and 16 indicate that actual data-model systematic *errors* are rather small, highly-localized on y_t and closely-correlated on n_{ch} . As noted above, TCM data descriptions are not obtained by fits to individual spectra. The Z-scores in those figures suggest that the systematic errors presented in Tables 3 and 4 of Ref. [4] greatly *overestimate* the uncertainties relevant to data description by an appropriate model.

B. Sensitivity to BW fit ranges

A particular issue for BW model fits is the p_t or y_t intervals over which fits to data are imposed. Fit ranges are determined by “the available data at low p_T ” (i.e. the effective particle acceptance lower cutoff) and “the agreement with the data at high p_t , justified considering that the assumptions underlying the blast-wave model *are not expected to be valid at high p_T* ” [emphasis added]. That policy begs the question where, if anywhere, is the BW model valid and by what criteria? Parameter systematic uncertainties are assigned empirically based on range variations: “The [fit] results are reported in Tab. 5 and Fig. 6. Variations of the fit range[s] lead to large shifts ($\sim 10\%$) of the fit results (correlated across centralities)....” What criteria are invoked to determine such variations?

Concerning utility of BW fits there is also the statement “It has be be kept in mind, however, that the actual values of the fit parameters depend substantially on the fit range. In spite of this limitations [sic], the blast-wave model still provides a handy way to compare the transverse momentum distributions and their evolution in different collision systems.” The statement apparently refers to BW fits to *individual* hadron species over the *entire* y_t acceptance as they appear in Fig. 1 of Ref. [4]. The quality of those data descriptions is not reported, and the parameter values are presumably meaningless based on the argument for limiting fit ranges above (“...not expected to be valid at high p_T ”). As to convenient data representation the variable-TCM description in Fig. 1 above describes all PID spectrum data within their statistical uncertainties *without relying on fits to individual spectra* and based on physically meaningful parameters.

C. Systematic vs statistical errors and Z-scores

As noted in Sec. V, Z-scores provide a superior *differential* measure of fit quality compared to the χ^2 statistic. Spectrum data associated with Ref. [4] include both statistical and systematic uncertainties. As noted in Sec. V C χ^2 values presented in Table 5 of Ref. [4] appear based on total systematic uncertainties rather than statistical uncertainties. That is one reason to question interpretation of such χ^2 values. Another is the practice to limit model-fit p_t intervals to what will provide a “good” fit, perhaps as determined by resulting χ^2 values.

An example of Z-score usage as standard practice for particle physics analysis can be found in Ref. [40] reporting properties of hadronic Z decays from the LEP. In its Fig. 1 appears “the difference between the distributions of the QCD models and the $[e^+e^-]$ data in units of the data error,” which is just the Z-score defined in Eq. (10). The “data error” here is “combined statistical and systematic errors.” Although that seems to correspond formally to χ^2 values in Ref. [4] the two uncertainty types have approximately the same magnitudes for the e^+e^- spectrum data in Fig. 20 below, in contrast to the factor ≈ 10 difference for spectrum data reported in Ref. [4].

Part of systematic uncertainty estimation relates to the *interpretability* of analysis results, but applies in this case to *model* uncertainty estimations themselves as opposed to data. If a statistic is employed to determine data-model agreement/disagreement do its resulting values provide a reliable evaluation of model validity? In the case of χ^2 values in Table 5 of Ref. [4] it is likely that the values reported are misleading, hence uncertain.

It can be argued that Z-scores should be calculated only with statistical uncertainties, which are usually unambiguous in a context where discrete objects are counted. Z-scores based solely on statistical uncertainties directly reveal systematic *errors* (as opposed to uncertainties) in both data and model. *Data* systematic errors are apparent for instance in Fig. 16 (b) (large narrow excursions) since the applied model (TCM) has no capacity to describe, and the collision process itself is unlikely to generate, such narrow structures. On the other hand, large and smooth deviations apparent in Fig. 13 (right) unambiguously reveal *model* systematic errors. A more effective venue for estimation of *systematic* model and data *errors* is differential Z-scores based on statistical uncertainties that are unambiguous in their definition.

VIII. DISCUSSION: TWO CULTURES

The blast-wave model represents one of two “cultures” relating to the dynamics of high-energy nuclear collisions, associated with a hydrodynamics- or hadronic-fluid-based description (flows) on the one hand and a particle or high-energy physics (partons) version of QCD on the other. As noted in Sec. VI A the former has its origins in the nuclear theory of Landau [28] (1950s) and ele-

ments of the fireball description of Hagedorn [29] (1960s) which substantially predate the experimental discovery of quarks and development of QCD theory (1970s) at which point it became evident that parton cascades or showers play a major role in high-energy collision dynamics.

A. Parton splitting cascades or showers

One of the most popular Monte Carlo models of elementary collisions is PYTHIA [41, 42]: “The [PYTHIA] program is designed to simulate the physics processes that can occur in collisions between high-energy particles, e.g. at the LHC collider at CERN. ... A combination of perturbative results and models for semihard and soft physics ... are combined to trace the evolution towards complex [e.g. hadronic] final states.” Initial developments that led to the PYTHIA Monte Carlo – “reproducing the work of Field and Feynman, and extending it to the analytical model developed in Lund” – were motivated by an early model of jet formation reported in Refs. [43–45]. “The ‘jets’ observed in both cases $[e^+e^-]$ and $p-p$ collisions] are thought to arise from *quarks that fragment or cascade into a collection of hadrons moving in roughly the direction of the original quark* [emphasis added]” [45].

Concerning early development of detailed mechanisms “Both of these [early jet models other than PYTHIA] were based on the concept of independent fragmentation, wherein each of the q , \bar{q} and g jets are assumed to fragment symmetrically around a jet axis defined by the direction of the respective parton in the CM frame of the event. In Lund, instead another picture had been developed, string fragmentation. Here the connecting colour field is approximated by a massless relativistic string, with gluons represented by pointlike momentum-carrying ‘kinks’.” “PYTHIA lacked the parton showers that gave the other two programs [ISAJET and FIELDJET] realistic jet shapes.” “It was clear that parton showers would play a key role in order to produce multijet final states...” [41].

Reference [41] notes that “...the soft-gluon emission pattern around a $q\bar{q}$ topology could be viewed as a sum of radiation off two independent dipoles...mimicking the nonperturbative string picture. ...this offered a starting point to formulate a [parton] shower as a successive branching [cascade] of dipoles, an idea that today is a standard choice for most shower algorithms...” In Ref. [46] a Lund Dipole Cascade model, implemented as the DIPSY Monte Carlo, is described: The model “gives a good description of inclusive pp and ep cross-sections (including diffraction), and a fair description of exclusive final states (min. bias and underlying event). The model can also be applied to reactions with nuclei, with some early results available.” In particular the model is able to describe η charge densities within $\eta \in [-2.5, 5]$ for 0.9 and 7 TeV $p\bar{p}$ collisions at the LHC. In summary, various Monte Carlo models based on parton splitting cascades

or showers are able to describe the hadronic final states of elementary (e^+e^- , p - p) collisions in considerable detail.

B. Hadron gas in thermodynamic equilibrium

An interesting alternative approach to e^+e^- collision data is reported in Ref. [47]. The study acknowledges that e^+e^- collisions (as an example) include both hard processes (parton showers) described by perturbative QCD and soft processes (parton fragmentation to hadron jets) that must be described phenomenologically, with the Jetset Monte Carlo (precursor to PYTHIA) as one example. Reference [47] comments: “The main unsatisfactory feature of these [Monte Carlo] models...is the large number of free parameters required in order to correctly reproduced experimental data. As a consequence, those models have a rather poor predictive power.”

The analysis assumes that “each jet [of an e^+e^- hadronic final state] represents an independent phase in complete thermodynamic equilibrium...” That assumption is taken to imply that “one can describe a jet as an object defined by thermodynamic and mechanical quantities such as temperature, volume...” The basis for analysis is “...the canonical partition functions of systems with internal symmetries.” The analysis is applied to final-state abundances of an array of hadron species. The study concludes that “...this model is able to fit impressively well the average multiplicities of light hadrons...” The model parameters are temperature T , volume V and γ_s related to strange-quark chemical equilibrium.

While that analysis is informative and technically competent it can be argued that “an independent phase in complete thermodynamic equilibrium” is not demonstrated by model agreement with hadron species abundances. In discussing the statistical properties of hadrons emerging from “freezeout” of A-A collisions at the SPS Ref. [48] warns that “...this apparent ‘thermal’ equilibrium is a result of the decay process, the nature of which lies well beyond the statistical model which ‘merely’ captures the apparent statistical order, prevailing right after decay. ... The observed equilibrium is, thus, *not achieved by inelastic transmutation of the various hadronic species densities, in final hadron gas rescattering cascades*, i.e. not by hadron rescattering approaching a dynamical equilibrium [emphasis added].” One may argue by analogy that the partons within a jet do not rescatter so as to achieve thermodynamic equilibrium prior to hadronization. It is the hadronization process itself, as a quantum transition following a least-action principle, that leads to approximate agreement with the description in Ref. [47].

The array of species abundances among jet fragments from e^+e^- collisions (what is addressed by Ref. [47]) is only part of the information carried by the fragment distribution from a jet ensemble. Single-particle momentum distributions and *multiparticle correlations* (on angle [49, 50] and p_t or y_t [51]), as well as *local* correlations among charge, flavor and baryon number, clearly indicate

that jets are not featureless equilibrated gases. In summary, while thermal equilibrium of a phase might imply a certain data profile, observation of such a data profile by experiment does not demonstrate thermal equilibrium.

C. Hadron emission from a flowing source

Within a parton cascade the initial momentum of a single leading particle is distributed by splitting to a shower of lower-momentum particles. Transfer of momentum to final-state hadrons can be described as *top-down*. In contrast, within a fluid-dynamics picture of high-energy collisions the initial projectile energy is to some extent “stopped” in the CM leading to high energy densities and pressure gradients that drive fluid flow. The resulting flow field, convoluted with a locally-isotropic Boltzmann distribution (Cooper-Frye formalism [5]), is expected to describe final-state momenta of emitted hadrons. Transfer of momentum/energy can be described as *bottom-up*.

Reference [52] discusses A-A collision dynamics at the LHC in the context of the Landau hydrodynamic model of high-energy nuclear collisions: “Consider first the case of central AA collisions with $A \gg 1$ such that nucleons of one nucleus collide with a large numbers of nucleons of the other nucleus and the *whole energy content* is used in particle production. This is the case of ‘*full stopping*’ [emphasis added]. ... Common to both Landau hydrodynamics and Bjorken hydrodynamics is the basic assumption that in the [conjectured] dense hot matter produced in high-energy heavy-ion collisions, the density of the quanta of the medium is so high that a state of local thermal equilibrium can be maintained through out.” The large densities imply corresponding large density *gradients* that drive flows. In such models much of the hadron momentum originates solely from pressure-induced flows combined with thermal emission. Any small jet contribution is assumed restricted to limited p_t intervals.

That is the context in which the BW model has been applied to particle data at the SPS and higher energies. Reference [1] asserts “In this paper we want to develop a phenomenological model for the hadronic matter by starting out with thermalization as the basic assumption and adding more features as they are dictated by the analysis of the measured hadronic spectra.” Referring to *nucleon* flows at the Bevalac is the statement “Though this directed flow [at the Bevalac] is of different nature as our collective expansion flow [at the SPS], it suggests the relevance of hydrodynamics also at higher energies.”

But there immediately appears evidence of conflict between such assumptions and what had emerged from high-energy (particle) physics study of elementary collisions. Reference [1] first admits that “Our current understanding of QCD results basically from high energy experiments with small collision systems [e.g. p - p collisions] suffering hard interactions which are relatively easy to analyse.” But given the similarity of β and p - p spectra at SPS energies Ref. [1] then argues that “It would

be too impulsive to deduce from the apparent similarity of pp and S+S spectra that the collective interpretation [i.e. flows in β] is wrong, since a) pp is by no means an elementary collision system which we understand in sufficient detail to serve as the antipode [opposite] of a collective system and b) only a few of the observed features of the [hadron] spectra can be fully reproduced by these two radically different philosophies which share only a small set of common principles as local energy-momentum conservation, relativistic space-time picture, etc.”

One may assume that “radically different philosophies” refers to “high energy experiments” and resulting parton-cascade descriptions (e.g. PYTHIA) on the one hand and a hydrodynamic approach implemented via a BW model on the other. If “pp is by no means an elementary collision system” then what is — e^+e^- ? Point a) above essentially excludes p - p collisions as a *reference* system for the study of A-B collisions although that has subsequently been common practice at the RHIC and LHC.

Concerning point b) is the statement “For other observables, which are not directly tied to the dynamics, e.g. strangeness, we already see a big enhancement compared to [minimum-bias] pp, thus indicating fundamental differences between both [S-S and p - p] collision systems.” But that conclusion can be strongly questioned in the context of measured *jet production* in p - p and for instance p -Pb collisions as reported in Refs. [6–8], in which minimum-bias jets are found to make strong contributions to strangeness and baryon production. The “fundamental differences” between β and p - p are more likely simply due to increased jet production in β collisions due to *multiple* N-N binary collisions (and hence increased jet production) *per nucleon participant* with otherwise no significant deviation from p - p observations.

In summary, descriptions of hadron emission from a flowing source, e.g. the BW model, compete directly with data descriptions in terms of parton cascades – within projectile nucleons leading to (soft) hadron distributions along the beam axis or within (hard) jets resulting from large-angle scattering of partons from projectile nucleons.

D. BW model compared with elementary collisions

It is informative to consider some examples of “elementary” collisions in comparison to model elements from the TCM. In particular, the $\sqrt{s_{NN}} = 19.4$ β spectrum data invoked in Ref. [1] are compared with 17 GeV (SPS) p - p data and with the soft-component model function that describes $\sqrt{s} = 200$ GeV p - p spectra [9]. These comparisons address in part the question: what is an elementary collision and how should it be modeled?

Figure 19 (left) shows a pion spectrum on m_t (solid dots, $2 \times \pi^-$) for SPS fixed-target 0-2% central β collisions at 200A GeV ($\sqrt{s_{NN}} = 19.4$ GeV) [53]. A hydro-model (BW) analysis of those data was used to infer radial flow with mean transverse speed $\langle \beta_t \rangle \rightarrow \tilde{\beta}_t \sim 0.25$ [1] (see Fig. 12, right, and associated text). The curve labeled

S_{NN} is the soft component for $\sqrt{s} = 200$ GeV NSD p - p collisions from the RHIC [9]. The line labeled M-B is the Boltzmann (exponential) limit of Lévy distribution S_{NN} with $T \approx 145$ MeV. A $\pi^+ + \pi^-$ spectrum from p - p collisions at 158A GeV (open circles, $\sqrt{s} = 17.3$ GeV) is included for comparison [54].

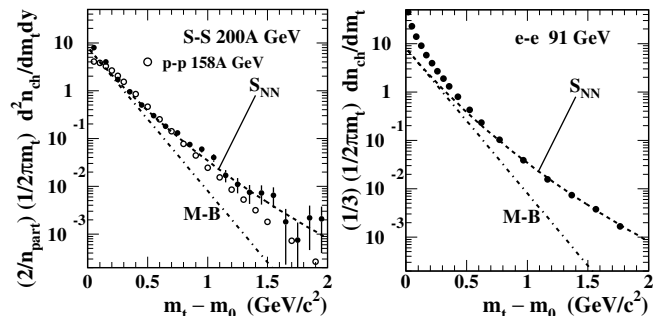


FIG. 19: Left panel: m_t spectra from 0-2% central β collisions at 200A GeV (solid points, $\sqrt{s_{NN}} = 19.4$ GeV) [53] and from p - p collisions at $\sqrt{s} = 17.3$ GeV (open circles) [54]. The dashed curve is Lévy soft component $\hat{S}_0(m_t)$ from 200 GeV p - p collisions. The dash-dotted curve is the Boltzmann limiting case of S_{NN} . Right panel: m_t spectrum (points) from e^+e^- collisions at $\sqrt{s} = 91$ GeV [40]. The curves are duplicated from the left panel. The e^+e^- data are rescaled as in the axis label to match the S_{NN} curve at larger m_t .

Fig. 19 (right) shows an m_t spectrum (points) from LEP e^+e^- collisions at $\sqrt{s} \approx 91$ GeV [40]. e^+e^- hadronic events from Z_0 decays are dominated by two-jet events (see Fig. 13 of Ref. [40]). The spectrum, derived from a sphericity analysis of $q\bar{q}$ dijets, reveals the jet fragment momentum distribution transverse to the thrust (dijet) axis. The LEP $dn_{ch}/p_t dp_t$ data were rescaled to overlap the p - p soft component S_{NN} (dashed curve), and hence the SPS β spectrum. The shape of the m_t spectrum from 91 GeV Z_0 decays is consistent with the soft component of p - p spectra at 200 GeV and the spectrum from central 19 GeV β collisions. Commonality of the soft-component shape (Lévy distribution) across energies and collision systems suggests that the TCM soft component is a universal feature of fragmentation for any leading particle – be it parton or hadron.

While the comparison in Fig. 19 (right) provides a hint of the relation among dijet formation in e^+e^- collisions, the hadronic final state of A-B nuclear collisions and the BW model a more direct comparison can be made.

Figure 20 (left) shows the e^+e^- p_t spectrum from Fig. 19 (right) replotted on y_t (derived from measured p_t assuming all hadrons are pions as for y_z below). The points are published dn_{ch}/dp_t data (Fig. 18a of Ref. [40]) divided by p_t with no other scaling. According to Ref. [40] this is the “charged particle momentum component transverse to the sphericity [dijet] axis and projected into the event plane.” The solid curve is a Lévy distribution on m_t [i.e. $\hat{S}_0(m_t)$] with slope parameter $T = 90$ MeV and Lévy exponent $n = 7.8$. Dashed curves show the effect of varying T by 10 MeV. For com-

parison, soft-component $\hat{S}_0(y_t)$ for pions in Fig. 1 (a) has $T = 145$ MeV and $n = 8.5$. The e^+e^- data are described within their published uncertainties except for the lowest three points at 0.02, 0.07 and 0.13 GeV/c.

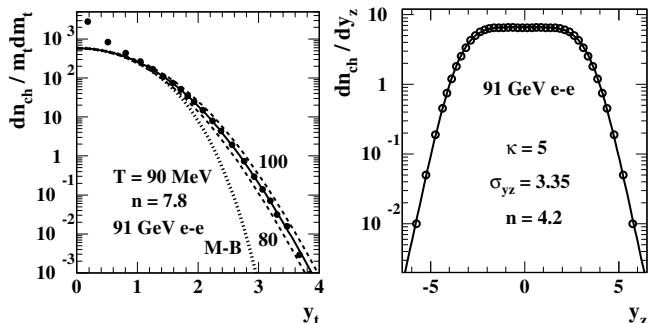


FIG. 20: Left: The hadron distribution on y_t (perpendicular to the dijet axis) from 91 GeV e^+e^- collisions [40]. The solid curve is a Lévy distribution [i.e. $\hat{S}_0(y_t)$] with parameters (T, n) noted in the figure. The dashed curves correspond to variation of T by 10 MeV. Dotted curve M-B is the exponential (on m_t) limit for $n \rightarrow \infty$ and $T = 90$ MeV. Right: Hadron distribution on y_z (parallel to the dijet axis) from 91 GeV $e^+e^- \rightarrow q\bar{q}$ collisions. The curve is Eq. (22) explained in the text.

Figure 20 (right) shows a hadron distribution on y_z from Z decays reported by Ref. [40]. y_z (y_s in Fig. 16a of Ref. [40] with s for “sphericity”) is derived from measured $p_L \rightarrow p_z$ along the event sphericity (dijet) axis and is based on assigning the pion mass to all hadrons. The solid curve is a generalized q -Gaussian distribution

$$G(y_z) = \frac{A}{[1 + (|y_z|/\sigma_{y_z})^\kappa/n]^n} \quad (22)$$

$$\sim A \exp_q[-(|y_z|/\sigma_{y_z})^\kappa],$$

with $\kappa = 5$, $\sigma_{y_z} = 3.35$, $n = 4.2$ and $A = 6.6$. The distribution differs from a Gaussian in two ways: (a) the parameter value $\kappa = 5$ rather than 2 leads to a more rectangular distribution and (b) the parameter value $n = 4.2$ controls the distribution tails. The q in “ q -Gaussian” refers to the relation $q - 1 = 1/n$. For $n \rightarrow \infty$ (and $\kappa = 2$) the distribution reverts to a standard Gaussian form. The kinematic limits of the data distribution are $y_z \approx \pm 6.5$ (for pions) corresponding to $\sqrt{s}/2 \approx 46$ GeV. The “ $1/e$ ” points at ± 3.35 correspond to 2 GeV/c.

Several issues are addressed by Figs. 12, 19 and 20:

Figure 12 demonstrates the relation between the commonly-applied BW model and (a) the Boltzmann distribution (agreement expected for $\hat{\beta}_t = 0$ by definition of BW model) and (b) $\hat{S}_0(y_t)$ inferred from spectrum data as the zero-density limit but requiring $\hat{\beta}_t \approx 0.25$ from the BW model to approximate the Lévy distribution.

Figure 19 demonstrates that the soft-component model (Lévy distribution) $\hat{S}_0(y_t)$ (S_{NN} in those figures) describes spectra from SPS p - p and S-S collisions and (for higher p_t) LEP e^+e^- collisions, all of which deviate strongly from a Boltzmann-distribution exponential for

reasons related to known QCD processes. The small difference between SPS *central* S-S spectra and p - p spectra may be due an expected jet contribution at $\sqrt{s_{NN}} \approx 19$ GeV [16]. The power-law tail of soft component $\hat{S}_0(y_t)$ inferred from 200 GeV p - p collisions is apparently able to approximate the jet contribution to the 19 GeV S-S spectrum, consistent with collision-energy dependence of the p - p soft component (see Ref. [23], Fig. 12 right).

Figure 20 reveals a direct connection between the TCM description of hadron-hadron collisions and e^+e^- collisions from LEP [40]. The left panel shows the p_t spectrum from e^+e^- collisions (solid dots) consistent in shape with soft component $\hat{S}_0(y_t)$ (solid curve) from p - p and p -Pb collisions. While the soft component for pions has $T \approx 145$ MeV that for e^+e^- collisions has the substantially lower value $T \approx 90$ MeV. Whereas the parton parents of final-state hadrons from A-B collisions experience Fermi motion within projectile nucleons and k_t contributions within a parton cascade the $q\bar{q}$ pair in a e^+e^- collision has *zero* transverse momentum in the CM frame leading to a “cooler” hadron fragment spectrum. On the other hand $n = 7.8$ for e^+e^- collisions represents a “harder” power-law tail for that spectrum than the $n = 8.5$ value for p - p collisions. Both observations are consistent with $\hat{S}_0(y_t)$, as the description *inferred from A-B data*, reflecting hadron production via parton splitting cascades within a conventional QCD context. The resulting Lévy data trend is *inconsistent* with the Boltzmann exponential trend assumed for the BW model.

Figure 20 (right) shows the complementary dijet fragment distribution on y_z (from Ref. [40] Fig. 16a) that can be compared with similar distributions on pseudorapidity from hadronic A-B collisions. Within a hydrodynamic model context such distributions are attributed within hadronic collisions to longitudinal flow or Bjorken expansion. Yet the very similar fragment distribution from e^+e^- collisions may be attributed to parton splitting cascades leading to dijets. In the first case longitudinal hadron momentum is attributed to pressure gradients, in the second case to a parton parent in the cascade carrying a fraction x of the leading-parton momentum. One description (flows) says that a particle has been pushed while another (partons) says that it has been “pulled.”

For both longitudinal and transverse momentum distributions from e^+e^- collisions the trend at higher momentum is a power law controlled by $n = 4.2$ for p_z and $n = 7.8$ for p_t , indicated by straight-line trends in Figure 20 on y_t or y_z . A similar power-law trend is observed for p_t spectrum hard components [e.g. Fig. 4 (b,d)] associated quantitatively in that case with large-angle-scattered partons fragmenting to jets [15].

Detailed study of p_t spectra from 5 and 13 TeV p - p collisions [55] demonstrates the two-component (projectile-proton dissociation and scattered parton fragmentation to dijets) nature of hadron production *consistent with basic QCD* in such “elementary” collisions. Statistical analysis of two models applied to the same data with intent to demonstrate thermalization and/or flows in p - p colli-

sions [56] are falsified via Z-score tests as in Sec. V. One might expect that “elementary” collisions (e^+e^- , p - p and even p -A systems) should be well understood after fifty years of theoretical and experimental QCD-related research whereas larger A-B collision systems might remain ambiguous. However, there seems to be a persistent tendency to assume that A-A collisions comprise the fixed reference and “elementary” collisions are seen as not elementary and still returning unanticipated results.

IX. SUMMARY

Hadron p_t spectrum analysis is a principal component of data interpretation relating to high-energy nuclear collisions. A major element of spectrum analysis is fitting models to spectrum data both as a form of data compression (reducing spectra to a few, possibly interpretable, parameters) and as a test of specific physical model predictions. Several models available for spectrum description are comprised of simple functions: (a) the Boltzmann exponential on transverse mass m_t , (b) the Tsallis model (“Tsallis statistics”) on m_t or p_t , (c) the blast-wave (BW) model on m_t and (d) the two-component (soft+hard) spectrum model (TCM). Also available are several complex Monte Carlo models (e.g. PYTHIA).

The BW model in particular, formulated to describe the effect on hadron momenta in the center-of-momentum frame of moving (flowing) particle sources, was intended to facilitate discovery of flows in A-A collisions as one manifestation of QGP formation. Early results from the relativistic heavy ion collider (RHIC) seemed to demonstrate flow manifestations in spectra.

More recently, the BW model as applied to p -A and even p - p collisions has been interpreted to support the same conclusions for small systems, although matter and energy densities achievable in such systems are *a priori* unlikely to produce a QGP. Such results cast doubt on the legitimacy of the BW model applied to collision data.

The present study of BW model applications to identified-hadron (PID) spectra from 5 TeV p -Pb collisions is a response to that situation. This study is intended to assess basic formulation(s) of the BW model and its (their) underlying assumptions, to determine data fit quality in relation to possible model falsification and to compare the BW model to alternative models that may provide superior data description and lead to different (and perhaps more credible) physical interpretations.

The general procedure includes the following steps: (a) visually compare BW model and TCM to data in basic semilog plots on transverse rapidity y_t where data trends have a particularly simple structure, (b) compare data and model *shapes* (what is emphasized in BW model applications) using model-independent measures, (c) assess data-model fit quality differentially and *quantitatively* using Z-scores, and (d) review BW model evolution across several decades via a number of published examples.

The specific results are as follows: (a) As established

in a previous study the TCM describes spectra for four hadron species within point-to-point uncertainties over the entire p_t acceptance and the TCM is *not* fitted to individual spectra. In contrast, the BW model fails to describe spectra except over limited p_t intervals *defined by data-model agreement*. That failure is most obvious for the case of pion spectra. (b) Data-model comparisons using model-independent methods (e.g. logarithmic derivatives) demonstrate qualitative differences between BW model and data. On that basis the model is falsified. (c) Application of the Z-score statistic, a standard measure of data-model agreement, demonstrates that the BW model is excluded as a spectrum model for this collision system, whereas the TCM is an acceptable model as established in a previous study. (d) While the general structure of the BW model is accepted, specific applications may be quite different in detail (what parameters are allowed to vary over what ranges, even basic algebraic structure) leading to difficulty in interpreting results.

If the BW model is accepted as a valid physical data model, albeit only within artificially-restricted p_t intervals (with doubtful justification), it is commonly concluded that the great majority of hadron production arises from a moving source exhibiting “collective” motion. However, the present study establishes that for the p -Pb collision system at 5 TeV the BW model is falsified by PID spectrum data. Previous studies have arrived at the same conclusion for 5 and 13 TeV p - p collisions.

In contrast, the TCM does provide a statistically-acceptable data description for *all* available PID spectrum data from 5 TeV p -Pb collisions. From that result the following conclusions may be drawn:

The TCM soft component is consistent with *nuclear transparency* (1976) wherein a projectile nucleon may transit a target nucleus intact, albeit “excited” (wounded nucleon model), with later dissociation to hadron fragments *outside* the collision space-time volume. That picture is consistent with the soft-component model *inferred from data* – a Boltzmann exponential with power-law tail indicating a heterogeneous source (e.g. parton shower).

The TCM hard component is quantitatively consistent with *minimum-bias dijet production* as represented by measured jet spectra and parton fragmentation functions. In that case final-state hadrons do indeed emerge from moving particle sources which however happen to be scattered partons as expected from basic QCD theory.

Appendix A: BW model derivation

Formulation of the BW model for single-particle momentum spectra requires evaluation of the integral [5]

$$E \frac{d^3 N}{dp^3} = \frac{g}{(2\pi)^3} \int_{\sigma} e^{-(u^\mu p_\mu)/T} p^\nu d^3 \sigma_\nu, \quad (\text{A1})$$

where a factor $\exp(\mu/T)$ is omitted. Evaluation requires determination of quantities $u^\mu(x)$, p_μ , σ_μ and $d^3 \sigma_\mu$,

where $u^\mu(x)$ is a fluid velocity field on space-time x in the CM or lab frame, p_μ is particle four-momentum in the lab frame and $\sigma(r\phi_x, \eta_s)$ is the volume (hypersurface) from which detected particles emerge (freeze out). The Boltzmann exponential assumes particle emission according to an isotropic thermal distribution in the local frame.

1. Basic four-vectors

The basic four-vectors required for evaluating Eq. (A1) are defined using a set of self-consistent symbols that overlap as much as possible the different conventions utilized in an assortment of relevant publications.

a. Space-time rapidity

The position four-vector in cylindrical coordinates preferred for large \sqrt{s} is

$$\begin{aligned} x_\mu &= [t, r, \phi, z] \\ &= [\tau \cosh(\eta_s), r \hat{e}(\phi_x), \tau \sinh(\eta_s)], \end{aligned} \quad (\text{A2})$$

where $\hat{e}(\phi_x)$ is a unit vector, with space-time rapidity

$$\eta_s \equiv \frac{1}{2} \ln \left(\frac{t+z}{t-z} \right) = \ln \left(\frac{t+z}{\tau} \right) \quad (\text{A3})$$

where $t = \tau \cosh(\eta_s)$, $z = \tau \sinh(\eta_s)$ and $v_s = \dot{z}/\dot{t} = \tanh(\eta_s)$. Azimuth angles in configuration and momentum spaces are distinguished by φ vs ϕ or ϕ_x vs ϕ_p , with the latter notation used below to reduce ambiguity. The space-time parameter ζ in Ref. [1] here goes to η_s .

Configuration-space rapidity η_s is distinguished from (a) momentum-space *pseudorapidity* η with no subscript and (b) longitudinal flow angle or boost η_z (in configuration space). Those distinctions are consistently maintained below unless explicitly noted. The approximation $\eta_z(z) \approx \eta_s(z)$ (Bjorken expansion) is often assumed. In what follows the two quantities are maintained distinct unless specifically noted otherwise.

b. Fluid (particle source) velocity field

Fluid velocity fields are distributed on configuration space x . The following are Lorentz hyperbolic (boost) angles for particle sources moving in the CM frame

$$\begin{aligned} \eta_t(r) &= (1/2) \ln \left(\frac{1+\beta_t}{1-\beta_t} \right) = \ln[\gamma_t(1+\beta_t)] \quad (\text{A4}) \\ \eta_z(z) &= (1/2) \ln \left(\frac{1+\beta_z}{1-\beta_z} \right) = \ln[\gamma_z(1+\beta_z)], \end{aligned}$$

with $\beta_x = \tanh(\eta_x)$, $\gamma_x = \cosh(\eta_x)$ and $\gamma_x^2 = 1/(1-\beta_x^2)$. Given those definitions the four-velocity field distributed

on configuration space is

$$\begin{aligned} u^\mu(x) &= \cosh(\eta_t) [\cosh(\eta_z), \tanh(\eta_t) \hat{e}(\phi_x), \sinh(\eta_z)] \\ &= \gamma_t [\gamma_z, \beta_t \hat{e}(\phi_x), \gamma_z \beta_z] \quad (\text{A5}) \\ u^\mu u_\mu &= 1 \end{aligned}$$

In Refs. [1, 22] $\rho \rightarrow \eta_t$ and $\eta \rightarrow \eta_z$ (“boost angles”) are functions of r and z respectively based on assumptions.

c. Particle momenta in the CM or lab frame

Given measured momenta in cylindrical coordinates (p_t, θ, ϕ) (e.g. in a solenoidal magnetic field) pseudorapidity $\eta = -\ln[\tan(\theta/2)]$ ($\sim y_z$ rapidity). The three-vector momentum is $p^\vec{r} = (p_x, p_y, p_z) = (p_t, \eta, \phi_p)$ with magnitude $p = p_t \cosh(\eta)$ and $p_z = p_t \sinh(\eta)$. Symbol η without subscript here always represents pseudorapidity.

Transverse mass m_t is defined by $m_t^2 = p_t^2 + m_0^2$. Transverse rapidity is $y_t = \ln[(m_t + p_t)/m_0]$ in a longitudinally comoving frame with $m_t = m_0 \cosh(y_t)$, $p_t = m_0 \sinh(y_t)$. Longitudinal rapidity is $y \rightarrow y_z = \ln[(E + p_z)/m_t]$ with $E = m_t \cosh(y_z)$, $p_z = m_t \sinh(y_z)$. With those definitions the particle four-momentum is

$$\begin{aligned} p_\mu &= [E, p_t \hat{e}(\phi_p), p_z] \quad (\text{A6}) \\ &= [m_t \cosh(y_z), p_t \hat{e}(\phi_p), m_t \sinh(y_z)] \\ &= m_t [\cosh(y_z), \tanh(y_t) \hat{e}(\phi_p), \sinh(y_z)] \\ p^\mu p_\mu &= m_0^2 \end{aligned}$$

d. Particle energy in the boost frame

With the velocity field for particle emission and the particle four-momentum defined the product represents particle energy in a conjectured boost frame based on measured particle momentum in the CM or lab frame [5].

$$\begin{aligned} u^\mu p_\mu &= \gamma_t m_t [\cosh(y_z) \cosh(\eta_z) - \sinh(y_z) \sinh(\eta_z)] \\ &\quad - \gamma_t \beta_t p_t \cos(\phi_x - \phi_p) \quad (\text{A7}) \\ &= \gamma_t [m_t \cosh(y_z - \eta_z) - \beta_t p_t \cos(\phi_x - \phi_p)] \\ &\rightarrow m_t \cosh(y_z) = E \quad \text{in the lab frame for no flows.} \end{aligned}$$

2. Emission hypersurface

The freezeout hypersurface σ appearing in Eq. (A1) is the configuration-space volume from which particles are emitted (decoupled from the source fluid) and then fly freely to a detector. In Ref. [5] the differential product $p^\mu d\sigma_\mu = (E - \beta p) dx = \bar{E} d\bar{x}$ for a 1D system, where bars denote quantities in the local, comoving or boost frame. That follows since $p_\mu = [E, p]$, $\sigma_\mu = [t, x]$, $d\sigma_\mu = [dx, dt]$ and $dt = \beta dx$ if $d\bar{t} = 0$. In what follows, several examples are presented for defining $d^3\sigma_\mu$ and determining $p^\mu d^3\sigma_\mu$.

a. Schnedermann et al. [1]

In this study the emission hypersurface (with $\zeta \rightarrow \eta_s$ the space-time rapidity, $\eta_s \in [-H_s, H_s]$ and $r \in [0, R]$) is

$$\sigma(r\phi_x, \eta_s) \rightarrow \sigma_\mu = [t(\eta_s), r\hat{e}(\phi_x), z(\eta_s)]. \quad (\text{A8})$$

The differential freezeout volume is then

$$d^3\sigma_\mu = \left[\frac{\partial z}{\partial \eta_s}, 0, 0, \frac{\partial t}{\partial \eta_s} \right] d\eta_s d\mathbf{d}\phi_x \quad (\text{A9})$$

assuming instantaneous freezeout in r , and with

$$p^\mu d^3\sigma_\mu = \left[E \frac{\partial z}{\partial \eta_s} - p_z \frac{\partial t}{\partial \eta_s} \right] d\eta_s d\mathbf{d}\phi_x. \quad (\text{A10})$$

The velocity field and four-momentum $u^\mu(x)$ and p^μ are as in App. A 1 b, with ‘‘boost angles’’ $\eta \rightarrow \eta_z(z)$ and $\rho(r) \rightarrow \eta_t(r)$ and with longitudinal momentum $p_L \rightarrow p_z$. Azimuth angles are $\varphi \rightarrow \phi_p$ and $\phi \rightarrow \phi_x$. If $z = \tau \cosh(\eta_s)$ and $t = \tau \sinh(\eta_s)$, with $E = m_t \cosh(y_z)$ and $p_z = m_t \sinh(y_z)$, then

$$p^\mu d^3\sigma_\mu \rightarrow m_t \tau \cosh(y_z - \eta_s) d\eta_s d\mathbf{d}\phi_x. \quad (\text{A11})$$

b. Tomasik et al. [35]

In this study the single-particle momentum spectrum is defined in terms of a ‘‘source function’’ $S(xp)$

$$E \frac{d^3N}{dp^3} = \int d^4\mathcal{S}(xp). \quad (\text{A12})$$

The source function is defined by

$$S(xp) d^4x \propto m_t \tau \cosh(y_z - \eta_s) e^{-u^\mu(x)p_\mu/T} \times G(r) H(\eta_s) d\eta_s d\mathbf{d}\phi_x \quad (\text{A13})$$

with $y \rightarrow y_z$, $\eta \rightarrow \eta_s$ and $\varphi \rightarrow \phi_x$. The function $H(\eta_s)$ is a Gaussian with width $\Delta\eta_s$. The function $G(r)$ is Gaussian with width R_G or flat over $r \in [0, R_B]$. A unit-normal Gaussian on τ is assumed integrated to yield mean value τ . The emission hypersurface is defined by

$$\sigma_\mu = [\tau \cosh(\eta_s), r\hat{e}(\phi_x), \tau \sinh(\eta_s)] \quad (\text{A14})$$

with (assuming $d\tau = 0$)

$$d^3\sigma_\mu = \tau [\cosh(\eta_s), 0, 0, \sinh(\eta_s)] d\eta_s d\mathbf{d}\phi_x. \quad (\text{A15})$$

Four-vectors u_μ and p_μ are as in App. A 1 b, with flow angles $\eta_l \rightarrow \eta_z(z)$ and $\eta_t(r)$ as above in Eq. (A4). Factors $m_t \tau \cosh(y_z - \eta_s)$ in Eq. (A13) result if $d^3\sigma_\mu$ defined above is combined with p_μ as in App. A 1 b. Note that here $\eta_t(r) = \tanh(\beta_t) \propto r$ instead of $\beta_t \propto r$ as in Ref. [1].

c. Florkowski and Broniowski Ref. [36]

In this study the emission hypersurface (with $\alpha_{||} \rightarrow \eta_s$ introduced as the space-time rapidity) is

$$\sigma_\mu = [\tau(\zeta) \cosh(\eta_s), \rho(\zeta) \hat{e}(\phi_x), \tau(\zeta) \sinh(\eta_s)], \quad (\text{A16})$$

where $\zeta \in [0, 1]$ is here simply a parameter that correlates proper time τ and radius ρ , not space-time rapidity η_s . The associated volume element (with $\phi \rightarrow \phi_x$) is

$$d^3\sigma^\mu = \left[\frac{\partial \rho}{\partial \zeta} \cosh(\eta_s), \frac{d\tau}{d\zeta} \hat{e}(\phi_x), \frac{d\rho}{d\zeta} \sinh(\eta_s) \right] \times \tau(\zeta) d\zeta \rho(\zeta) d\eta_s d\phi_x. \quad (\text{A17})$$

The velocity field $u_\mu(x)$ [with $\alpha_\perp(\zeta) \rightarrow \eta_t(\zeta)$] is consistent with Eq. (A5) except $\alpha_{||} \rightarrow \eta_z$ (boost angle), not η_s (space-time rapidity), and an error in factorization has been corrected. Particle momentum p_μ is consistent with App. A 1 b if $m_\perp \rightarrow m_t$, $y \rightarrow y_z$ and $\varphi \rightarrow \phi_p$. In that case

$$p^\mu d^3\sigma_\mu = \left[m_t \cosh(y_z - \eta_s) \frac{\partial \rho}{\partial \zeta} - p_t \cos(\phi_p - \phi_x) \frac{d\tau}{d\zeta} \right] \times \rho(\zeta) \tau(\zeta) d\zeta d\eta_s d\phi_x. \quad (\text{A18})$$

If one assumes $d\tau/d\zeta \rightarrow 0$ as in Ref. [36] and $\rho \rightarrow r$ then

$$d^3\sigma_\mu \rightarrow \tau [\cosh(\eta_s), 0, 0, \sinh(\eta_s)] d\eta_s d\mathbf{d}\phi_x \quad (\text{A19})$$

which is consistent with Eq. (A15), and

$$p^\mu d^3\sigma_\mu \rightarrow m_t \tau(\zeta) \cosh(y_z - \eta_s) d\eta_s r(\zeta) d\mathbf{d}\phi_x. \quad (\text{A20})$$

To clarify, the distinction between space-time rapidity and longitudinal boost angle for Ref. [36] is as follows: $\alpha_{||}$ is initially introduced as space-time rapidity ($\rightarrow \eta_s$). But α_\perp is then initially introduced as transverse boost angle ($\rightarrow \eta_t$) with transverse flow $v_r \rightarrow \beta_t = \tanh \eta_t$, and $\alpha_{||}$ is later reintroduced as longitudinal boost angle ($\rightarrow \eta_z$) with longitudinal flow $v_z \rightarrow \beta_z = \tanh(\eta_z)$. The initial assumption is that $\eta_s \approx \eta_z$ with $\alpha_{||}$ filling both roles. In this appendix space-time η_s and velocity-field η_z are maintained distinct unless indicated otherwise.

d. Rath et al. [22]

In this study u_μ and p_μ are as in App. A 1 b with $\eta \rightarrow \eta_z$ (longitudinal flow angle), $\rho \rightarrow \eta_t$, $y \rightarrow y_z$, $\phi \rightarrow \phi_p$ and $\phi_r \rightarrow \phi_x$. $d^3\sigma_\mu$ is as in Eq. (A15) except $\eta \rightarrow \eta_s$ (space-time rapidity) and with a minus sign corrected. With those definitions

$$\begin{aligned} p^\mu d^3\sigma_\mu &= m_t \tau [\cosh(y_z) \cosh(\eta_s) - \sinh(y_z) \sinh(\eta_s)] \\ &\quad \times d\eta_s d\mathbf{d}\phi_x \\ &= m_t \tau \cosh(y_z - \eta_s) d\eta_s d\mathbf{d}\phi_x \end{aligned} \quad (\text{A21})$$

and

$$u^\mu p_\mu = \gamma_t [m_t \cosh(y_z - \eta_z) - \beta_t p_t \cos(\phi_x - \phi_p)]. \quad (\text{A22})$$

The ‘‘Bjorken correlation in rapidity’’ is specified as ($y \approx \eta$) \rightarrow ($y_z \approx \eta_s$) rather than the conventional $\eta_z \approx \eta_s$. That assignment of y_z is incorrect [see Eq. (A21)].

In summary, the above examples illustrate the differences and similarities among several approaches to the BW model over nearly thirty years, from 1993 to 2020.

3. Single-particle spectra and blast-wave model

The several definitions of relevant quantities in the previous subsections are combined to evaluate Eq. (A1) with

$$E \frac{d^3 N}{dp^3} = \frac{d^3 N}{m_t dm_t dy_z d\phi_p}. \quad (\text{A23})$$

For each case in App. A 2 Eq. (A1) is evaluated with the relevant quantities and consistent symbols adopted herein. Distinction between longitudinal flow angle η_z and space-time rapidity η_s is maintained unless stated otherwise. But just as $\beta_t(r) = \tanh^{-1}(\eta_t) \sim r$ is often assumed $\beta_z(z) = \tanh^{-1}(\eta_z) \sim z$ may also be assumed in the form of Bjorken expansion $\eta_z(z) \approx \eta_s = \ln[(t+z)/\tau]$.

a. Schnedermann et al. [1]

The formulation in Eq. (14) of Ref. [1] is modified by $\zeta \rightarrow \eta_s$, $\mathcal{Z} \rightarrow H_s$, $y \rightarrow y_z$, $\rho \rightarrow \eta_t$, $\eta \rightarrow \eta_z$ and invoking the expression in Eq. (A11), in which case

$$\begin{aligned} E \frac{d^3 N}{dp^3} &= \frac{g}{(2\pi)^3} m_t \tau \int_{-H_s}^{H_s} d\eta_s \cosh(y_z - \eta_s) \quad (\text{A24}) \\ &\times \int_0^R dr \exp[-m_t \cosh(\eta_t) \cosh(y_z - \eta_z)/T] \\ &\times \int_0^{2\pi} d\phi_x \exp[p_t \sinh(\eta_t) \cos(\phi_x - \phi_p)/T]. \end{aligned}$$

For the integrations, integrals over ϕ_p and ϕ_x give factor $(2\pi)^2 I_0 [p_t \sinh(\eta_t)/T]$. Then $\cosh(y_z - \eta_s) \rightarrow \cosh(y_z - \eta_z) \cosh(\eta_z - \eta_s)$, omitting the odd term $\sinh(y_z - \eta_z) \sinh(\eta_z - \eta_s)$ that will not contribute to the y_z integral. Both sides are integrated over longitudinal rapidity y_z leading to factor $2K_1 [m_t \cosh(\eta_t)/T]$. The integral over η_s then yields a constant no matter what the relation between η_s and η_z , although equality (Bjorken expansion) is usually assumed in which case the integral over $\eta_s \rightarrow 2H_s$ ($= 2Z_t$ in Ref. [1]). The result, assuming $\eta_t(r) \sim r$, is

$$\begin{aligned} \frac{dN}{m_t dm_t} &\approx \frac{g}{\pi} m_t \tau 2H_s \times \quad (\text{A25}) \\ &\int_0^R dK \quad {}_1[m_t \cosh(\eta_t)/T] I_0 [p_t \sinh(\eta_t)/T] \end{aligned}$$

near midrapidity ($y_z \approx 0$) which agrees with Eq. (14) of Ref. [1] except for the factor τ . $\beta_r(r) \rightarrow \beta_t(r) = \beta_s(\not{r}R)^n$ with $\beta_t = \tanh(\eta_t)$ is assumed with $n = 2$. It is observed that ‘‘the form of the profile [i.e. value of n] is not important for the [data] analysis.’’ But results in Fig. 11 (c) demonstrate that parameter n does strongly affect the BW model above $y_t \approx 1.8$ ($p_t \approx 0.4$ GeV/c).

b. Tomásik et al. [35]

In this study explicit model functions on η_s , r and τ are introduced to define the emission space-time volume. The integrals in Eq. (A24) then become (with $\eta \rightarrow \eta_s$ and omitting factor $e^{\mu/T}$)

$$\begin{aligned} E \frac{d^3 N}{dp^3} &= \frac{1}{(2\pi)^3} m_t \tau \int_{-\infty}^{\infty} d\eta_s H(\eta_s) \cosh(y_z - \eta_s) \\ &\times \int_0^{\infty} d\mathcal{G} (r) \exp[-m_t \cosh(\eta_t) \cosh(y_z - \eta_z)/T] \\ &\times \int_0^{2\pi} d\phi_x \exp[p_t \sinh(\eta_t) \cos(\phi_x - \phi_p)/T], \quad (\text{A26}) \end{aligned}$$

where an additional integral over τ is simply represented by mean value τ above. It is noted that the longitudinal rapidity or flow angle $\eta_l(x) \rightarrow \eta_z(x)$ is identified with space-time rapidity η_s such that longitudinal speed $\beta_z = \tanh(\eta_z) \rightarrow \tanh \eta_s = \not{z}t$. That is analogous to a common transverse prescription $\beta_t(r) = \beta_s(\not{r}R)^n$, in this case with $n = 1$. However, in this study the adopted *transverse* relation is $\eta_t(x) = \eta_f(\not{r}r_{rms})$. The integrals over ϕ_p and ϕ_x should give the same result as in the previous case. However, if there is no integration over y_z the integrals over η_s and r may require numerical techniques.

c. Florkowski and Broniowski Ref. [36]

In this study the single-particle spectrum is expressed as (omitting factor $e^{\mu/T}$ and including $d\phi_p$ at left)

$$\begin{aligned} \frac{d^3 N}{d^2 p_t dy_z d\phi_p} &= \frac{1}{(2\pi)^3} \int_0^{2\pi} d\phi_x \int_{-\infty}^{\infty} d\eta_s \int_0^1 d\zeta \rho(\zeta) \tau(\zeta) \\ &\times \left[m_t \cosh(y_z - \eta_s) \frac{d\rho}{d\zeta} - p_t \cos(\phi_x - \phi_p) \frac{d\tau}{d\zeta} \right] \quad (\text{A27}) \\ &\times \exp[-m_t \cosh(\eta_t) \cosh(y_z - \eta_z)/T] \\ &\times \exp[p_t \sinh(\eta_t) \cos(\phi_x - \phi_p)/T]. \end{aligned}$$

The final result assumes that $d\tau/d\zeta \rightarrow 0$, in which case $d\zeta \rho(\zeta) \tau(\zeta) d\rho/d\zeta \rightarrow \tau(r) dr$ with presumably $r \in [0, R]$ for some R . The integrals over $\varphi \rightarrow \phi_p$ and $\phi \rightarrow \phi_x$ should then give the same result as in the previous cases. If $\eta_z \rightarrow \eta_s$ (assumed Bjorken expansion) then the integral over $\alpha_{||} \rightarrow \eta_s$ gives $2K_1 (m_t \cosh(\eta_t)/T)$ as above. The further assumption is made that $\alpha_{\perp}(\zeta) \rightarrow \eta_t(r)$ is constant, in which case the integral over $\zeta \rightarrow r$ gives $\bar{\tau} R^2/2$.

If that assumption is dropped the result is

$$\frac{d^2 N}{m_t dm_t dy_z} = \frac{1}{\pi} m_t \quad (\text{A28})$$

$$\times \int_0^R \tau(r) d\mathcal{K}_1 [m_t \cosh(\eta_t)/T] I_0 [p_t \sinh(\eta_t)/T],$$

which can be compared with Eq. (A25).

d. Rath et al. [22]

Reference [22] assumes u_μ, p_μ and $d^3\sigma_\mu$ as in App. A 1 and Eq. (A15) with $\eta_z \rightarrow \eta_s$ (space-time rapidity), arriving at the single-particle distribution

$$\frac{d^2 N}{dp_T dy} \propto \int_0^{R_0} d\mathcal{K}_1 \left(\frac{m_T \cosh \rho}{T_{kin}} \right) I_0 \left(\frac{p_T \sinh \rho}{T_{kin}} \right) \quad (\text{A29})$$

given the usual $\rho \rightarrow \eta_t$ and $y \rightarrow y_z$. It is further assumed that $y = \eta \rightarrow y_z = \eta_s$ reflects Bjorken expansion which is incorrect, and given the prior assumption $\eta_z \rightarrow \eta_s$ this further assumption is unnecessary. The “flow profile” function $\beta_t(r)$ is as for Eq. (A25) but with $n = 1$. A substantial problem for Eq. (A29) is missing factors $p_t m_t$ or m_t^2 compared for instance with Eq. (A28).

e. Lao, Liu and Ma [38]

In this study the single-particle momentum distribution is derived from Eq. (3.1) in Ref. [35] via Eq. (18)

in Ref. [37] (omitting factor $e^{\mu/T}$ and $\hbar \rightarrow 1$) with e.g. $\eta_{smax} \rightarrow H_s$ as

$$E \frac{d^3 N}{dp^3} = \frac{1}{(2\pi)^2} m_t \tau \int_{-H_s}^{H_s} d\eta_s H(\eta_s) \cosh(y_z - \eta_s)$$

$$\times \int_0^\infty d\mathcal{G}(r) \exp[-m_t \cosh(\eta_t) \cosh(y_z - \eta_z)/T]$$

$$\times I_0 [p_t \sinh(\eta_t)/T]. \quad (\text{A30})$$

In Ref. [37] $y_z = 0$ is assumed (near midrapidity) and therefore does not appear in its Eq. (18). In Ref. [38] y_z is retained but $\cosh(y_z - \eta_s) \rightarrow \cosh(y_z) \cosh(\eta_s)$ with the $\sinh(y_z) \sinh(\eta_s)$ term omitted. The expression is further simplified by taking $G(r) \rightarrow 1$ (with $r \in [0, R]$) and $H(\eta_s) \rightarrow 1$ in which case Eq. (A30) is reduced to Eq. (A24) (after integration over ϕ_x). In that case integration over η_s should result in Bessel function $K_1 [m_t \cosh(\eta_t)/T]$. However, for their Eq. (4) it is decided to set $\eta_s = 0$ (“single source emission”), and the Bessel function must be replaced by $\cosh(y_z) \exp[-m_t \cosh(y_z) \cosh(\eta_t)/T]$ which near midrapidity ($y_z \approx 0$) is in effect a Boltzmann distribution with radially varying $T(r)$. That expression then represents the BW model as it is applied to data spectra.

-
- [1] E. Schnedermann, J. Sollfrank and U. W. Heinz, Phys. Rev. C **48**, 2462 (1993).
- [2] K. Adcox *et al.* (PHENIX) Phys. Rev. C **69**, 024904 (2004).
- [3] B. I. Abelev *et al.* (STAR), Phys. Rev. C **79**, 034909 (2009).
- [4] B. B. Abelev *et al.* [ALICE Collaboration], Phys. Lett. B **728**, 25 (2014).
- [5] F. Cooper and G. Frye, Phys. Rev. D **10**, 186 (1974).
- [6] T. A. Trainor, arXiv:2112.09790 [hep-ph].
- [7] T. A. Trainor, arXiv:2112.12330 [hep-ph].
- [8] T. A. Trainor, J. Phys. G **47**, no.4, 045104 (2020).
- [9] J. Adams *et al.* (STAR Collaboration), Phys. Rev. D **74**, 032006 (2006).
- [10] W. Busza *et al.*, Phys. Rev. Lett. **34**, 836 (1975).
- [11] S. Chapman and M. Gyulassy, Phys. Rev. Lett. **67**, 1210-1213 (1991).
- [12] A. Bialas, M. Bleszynski and W. Czyz, Nucl. Phys. B **111**, 461 (1976).
- [13] T. A. Trainor and D. T. Kettler, Phys. Rev. D **74**, 034012 (2006).
- [14] T. A. Trainor, Int. J. Mod. Phys. E **17**, 1499 (2008).
- [15] T. A. Trainor, Phys. Rev. C **80**, 044901 (2009).
- [16] T. A. Trainor, Phys. Rev. D **89**, 094011 (2014).
- [17] T. A. Trainor, arXiv:1701.07866.
- [18] T. A. Trainor, arXiv:1801.05862.
- [19] B. B. Abelev *et al.* (ALICE Collaboration), Phys. Lett. B **727**, 371 (2013).
- [20] T. A. Trainor, arXiv:1708.09412.
- [21] J. Adam *et al.* (ALICE Collaboration), Phys. Rev. C **91**, no. 6, 064905 (2015).
- [22] R. Rath, A. Khuntia, R. Sahoo and J. Cleymans, J. Phys. G **47**, no.5, 055111 (2020).
- [23] T. A. Trainor, J. Phys. G **44**, no. 7, 075008 (2017).
- [24] G. Wilk and Z. Włodarczyk, Nucl. Phys. B Proc. Suppl. **75**, no.1-2, 191-193 (1999).
- [25] G. Wilk and Z. Włodarczyk, Phys. Rev. Lett. **84**, 2770 (2000).
- [26] S. Acharya *et al.* (ALICE), Eur. Phys. J. C **80**, no.8, 693 (2020).
- [27] E. Kreyszig (1979). *Advanced Engineering Mathematics* (Fourth ed.), Wiley, p. 880, eq. 5.
- [28] L. D. Landau, Izv. Akad. Nauk SSSR **17**, 51 (1953).
- [29] R. Hagedorn, Nuovo Cimento Suppl. **3** 147 (1965).
- [30] R. Hagedorn, Nuovo Cim. A **52**, no.4, 1336-1340 (1967). ORPHAN
- [31] P. J. Siemens and J. O. Rasmussen, Phys. Rev. Lett. **42**, 880 (1979).

- [32] H. A. Gustafsson, H. H. Gutbrod, B. Kolb, H. Lohner, B. Ludewigt, A. M. Poskanzer, T. Renner, H. Riedesel, H. G. Ritter and A. Warwick, *et al.* Phys. Rev. Lett. **52**, 1590-1593 (1984).
- [33] P. Danielewicz and G. Odyniec, Phys. Lett. B **157**, 146-150 (1985).
- [34] C. Cesarotti, M. Reece and M. J. Strassler, JHEP **07**, 215 (2021).
- [35] B. Tomásik, U. A. Wiedemann and U. W. Heinz, Acta Phys. Hung. A **17**, 105-143 (2003).
- [36] W. Florkowski and W. Broniowski, Acta Phys. Polon. B **35**, 2895-2910 (2004).
- [37] R. L. Ray and A. Jentsch, Phys. Rev. C **99**, no.2, 024911 (2019).
- [38] H. L. Lao, F. H. Liu and B. Q. Ma, Entropy **23**, no.7, 803 (2021).
- [39] Z. Tang, Y. Xu, L. Ruan, G. van Buren, F. Wang and Z. Xu, Phys. Rev. C **79**, 051901 (2009).
- [40] D. Buskulic *et al.* (ALEPH Collaboration), Z. Phys. C **55**, 209 (1992).
- [41] T. Sjöstrand, Comput. Phys. Commun. **246**, 106910 (2020).
- [42] T. Sjöstrand, S. Mrenna and P. Z. Skands, Comput. Phys. Commun. **178**, 852-867 (2008).
- [43] R. D. Field and R. P. Feynman, Phys. Rev. D **15**, 2590-2616 (1977).
- [44] R. P. Feynman, R. D. Field and G. C. Fox, Phys. Rev. D **18**, 3320 (1978).
- [45] R. D. Field and R. P. Feynman, Nucl. Phys. B **136**, 1 (1978).
- [46] G. Gustafson, Acta Phys. Polon. B **42**, 2581-2606 (2011).
- [47] F. Becattini, Z. Phys. C **69**, no.3, 485-492 (1996).
- [48] R. Stock, arXiv:hep-ph/0312039 [hep-ph].
- [49] R. J. Porter and T. A. Trainor (STAR Collaboration), J. Phys. Conf. Ser. **27**, 98 (2005).
- [50] R. J. Porter and T. A. Trainor (STAR Collaboration), PoS C **FRNC2006**, 004 (2006).
- [51] M. Abdallah *et al.* (STAR), arXiv:2204.11661 [nucl-ex].
- [52] C. Y. Wong, EPJ Web Conf. **7**, 01006 (2010).
- [53] J. Baechler *et al.* (NA35 Collaboration), Phys. Rev. Lett. **72**, 1419 (1994).
- [54] C. Alt *et al.* (NA49 Collaboration), Eur. Phys. J. C **45**, 343 (2006).
- [55] T. A. Trainor, arXiv:2104.08423 [hep-ph].
- [56] T. A. Trainor, arXiv:2107.10899 [hep-ph].